GRAYSCALE PATTERNING OF PEDOT:PSS FILMS BY MULTIPHOTON LITHOGRAPHY

by

XIAO YAO

B.S., Hua Zhong Normal University, 2001

A THESIS

submitted in partial fulfillment of the requirements for the degree

MASTER OF SCIENCE

Department of Chemistry
College of Art and Science

KANSAS STATE UNIVERSITY
Manhattan, Kansas

2008

Approved by:

Major Professor
Daniel. A. Higgins

Abstract

Lithography techniques have been widely used to fabricate optical, electronic and optoelectronic devices with sub-micron scale spatial resolution. In the most common lithographic procedures, a light sensitive polymer, called a photoresist, is exposed and developed to form a binary relief pattern on a substrate. The finest features are produced by X-ray or electron-beam methods, both of which are very expensive to employ. Less expensive methods use ultraviolet (UV) light to expose the photoresist through a photomask. The resolution in these methods is somewhat lower and is governed by diffraction of light by the photomask, the quality of the photomaks, and by any chemical/physical development steps subsequently employed. Due to the above limitations, we have been investigating direct-write, ablative multiphoton lithography as an alternative method for preparing high-resolution patterns. With this method, near-IR light from an ultrafast pulsed laser source is focused into a polymer film, leading to depolymerization and vaporization of the polymer. Arbitrary binary patterns can be produced by raster scanning the sample while controlling exposure of the film to the laser. Importantly, high-resolution etching of the polymer film is achieved without the use of a photomask and without chemical development steps. While arbitrary patters are easily prepared, it is also possible to prepare three-dimensional (i.e. grayscale) surface relief structures.

In this study, ablative multiphoton photolithography is used to prepare binary and grayscale structures in thin films of PEDOT:PSS, an electrically conductive organic polymer blend. A simple kinetic model is proposed to explain the etching process. Data on the power-dependence of polymer etching can be fit to this model and is used to determine the order of the nonlinear optical process involved. The etch depth as a function of laser focus is also investigated and shown to follow the same kinetic model. The results show that three-dimensional (grayscale) patterns can be prepared by modulating either the laser power or the laser focus. Images of several binary and grayscale structures prepared by this method are presented.

Table of Contents

List of Figures

Acknowledgements

The author gratefully acknowledges financial support from the National Science Foundation (CHE-9709034, DMR-0076167 and CHE-0404578) and from Kansas State University. Thanks to everyone in Higgins group, especially Jeff Lange for helping with experimental setup. Special thanks to Dr. Daniel. A. Higgins for advising the experimental plan and modifying this manuscript.

Dedication

This work is dedicated to my family, including my grandparents, my parents and especially my husband.

CHAPTER 1 - Introduction to Optical Lithography

In this first chapter, background information of optical lithography will be introduced, followed by a thorough discussion of laser ablation lithography in polymer films, which is the technique employed in this thesis. The discussion will include the history of the technique, mechanisms and models, light sources for ablation, polymers that have been investigated, and the applications of these polymers. Finally, a short conclusion will be presented.

A wide variety of lithography systems exist which can be primarily categorized according to the type of radiation employed such as Optical, X-ray, E-beam and Ion beam. There is a large body of literature available for non-optical lithography, and the reader is referred to recent books and reviews on these methods[1-3]. Only optical lithography will be covered in this introductory chapter.

1.1 General Optical Lithography

1.1.1 Introduction to Methods

Optical lithography is a complicated process most commonly used to mass-produce patterned silicon wafers in integrated circuit manufacturing. "Optical", here, refers to a lithographic process that uses visible or ultraviolet light to form patterns on the photoresist. Patterning is accomplished by projecting an image of the pattern onto the photoresist film using a light source and a photo mask. Depending on the design of the photolithography machine, the mask may be in contact with the surface, very close to the surface or used to project onto the surface of the photoresist. These patterning methods are called contact, proximity, or projection respectively. Contact patterning is capable of attaining resolutions of less than 1 micron[4], but the presence of contact between the mask and the resist somehow diminishes the uniformity of attainable resolution across the wafer. This contact also results in defects in masks requiring regular disposal of masks after a certain level of use. Instead, in proximity and projection methods, no contact between the mask and the wafer is involved, which is why masks used with these techniques have longer lives than those used in contact methods. The resolution achieved by proximity method is not as good as that of contact method due to the diffraction of light. This

diffraction is caused by the light passing through slits that make up the pattern in the mask, and traversal across the gap between the mask and the wafer. The third technique, projection method, enlarges the gap between the mask and the wafer to get rid of the diffraction from proximity method. The resolution achieved by projection method depends on the wavelength and coherence of the incident light and the numerical aperture (NA) of the lens. This dependence will be discussed later in this chapter.

An example of a projection lithography system[5] commonly used in optical lithography is illustrated in Figure 1.1. In this system, ultraviolet light from a laser is first passed through an illuminator, which expands, homogenizes, and conditions the beam. It is then directed through the photomask, which contains the pattern to be imaged onto the wafer. The wafer is coated with a photosensitive material, the photoresist. For preparation of the smallest features, complex projection lens is then used to reduce the photomask pattern by a factor of four or five onto the photoresist. This kind of process is known as reduction projection lithography.

The performance of the projection system is ultimately determined by the laws governing the propagation of electromagnetic waves. In lithography, there are two key metrics: the resolution, which is the ability of the system to distinguish between nearby features, and the depth of focus, which is a measure of the precision with which the surface of the wafer must be positioned. Both quantities depend on the patterning wavelength λ and the numerical aperture (NA) of the lens, the latter being equal to $n\sin\theta$, where θ is the half-angle of the converging rays in the imaging system (see Figure 1.1) and n is the index of refraction of the medium in contact with the photoresist.

$$\text{Resolution} = \frac{k_1\lambda}{NA} \tag{1}$$

$$\text{Depth of focus} = \frac{k_2\lambda}{(NA)^2} \tag{2}$$

Where λ is the wavelength of the light source, NA is the numerical aperture of the lens, k_1 and k_2 are coefficients that encapsulate process-related factors. Equation (1) indicates that improved resolution can be obtained by reducing the wavelength λ of the laser and by increasing the NA of the imaging system. Continuous improvements in optical lithography have enabled the patterning of ever finer features, with smallest size, or critical dimension, decreasing by half

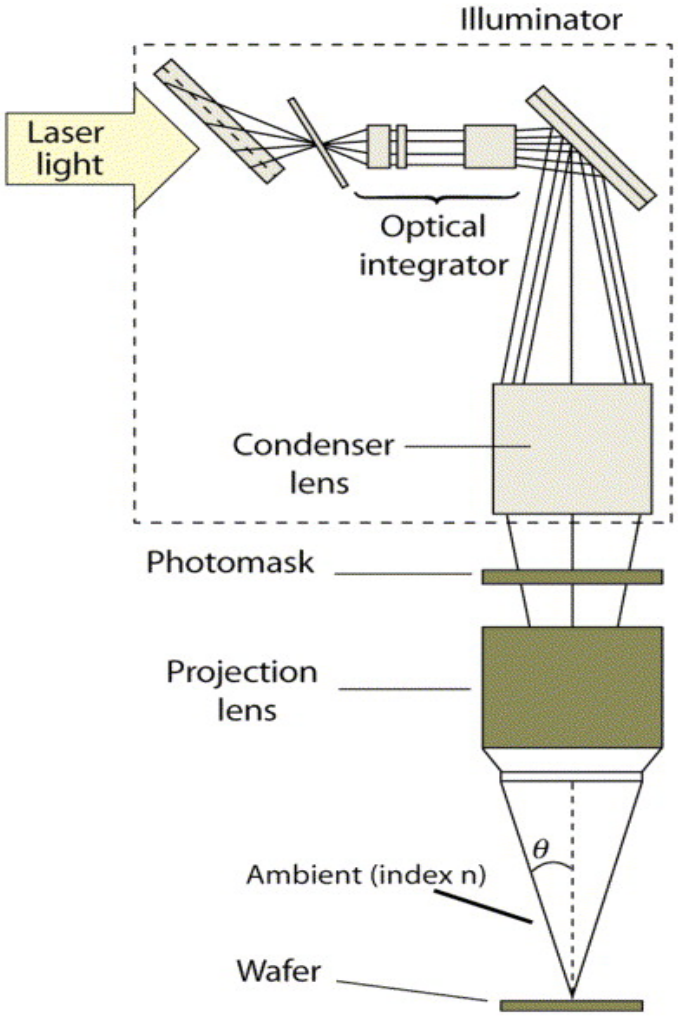

Figure 1.1 Scheme of the reduction projection lithography system. Main components are the laser, illuminator, photomask, projection lens and photoreist-coated wafer. Reprinted with permission from ref 5.

every eighteen months. This trend is known as Moore's law[6]. Keeping pace with Moore's law has been the main challenge of optical lithography over recent years. Lately this has involved addressing the complex technological challenge of using deep ultraviolet lasers and fabricating optics with very high NAs and near-diffraction-limited performance.

1.1.2 Emerging Methods for Optical Lithography

Keeping pace with Moore's law has led to the emergence of many new lithography techniques. Here, the recent advances in following emerging lithography techniques: Extreme Ultra-Violet Lithography (EUVL), Nano-Imprint Lithography (NIL), and Two-Photon, Three-Dimensional Lithography will be discussed.

EUVL, an extension of deep ultraviolet lithography, employs wavelengths below 100 nm for photoresist exposure. Since all matter absorbs EUV radiation, this method must be implemented in a vacuum. The current resolution of EUVL is 50 nm using a light source at 13 nm, and 20 nm resolution will be ultimately possible[7]. There are two major research directions specific to EUV lithography that are now receiving attention worldwide: light sources and reflective multilayer coatings. An important potential source of EUV light are laser-generated plasmas. Many experimental and theoretical studies[8,9] show that these sources can routinely achieve conversion efficiencies from laser energy to useful EUV energy of 1 - 2 %, depending on target and laser parameters. Also, the development of highly reflective Mo-Si multilayer coatings has been a key enabling technology for EUVL. With these coatings, reflectivities of greater than 63% are now routinely achieved at 13.4 nm[10].

The second technique introduced is Nano-Imprint Lithography (NIL), which can be used to produce structures as small as 25 nm over a large area with a high-throughput and at low-cost[11]. Two basic steps are performed during implementation of NIL. First, a mold with nanostructures on its surface is pressed into a thin resist film on a substrate, followed by removal of the mold. During this step, the resist is heated above its glass transition temperature, where it becomes a viscous liquid and can be readily deformed into the shape of the mold. The second step involves pattern transfer, where an anisotropic etching process is used to remove the residual resist in the compressed area. This step transfers the thickness contrast pattern into the entire resist. Unlike conventional lithographic methods, imprint lithography itself does not involve optical illumination, therefore its resolution is not limited by diffraction.

The final technique to be discussed is Two-Photon Three-Dimensional Lithography. The most promising results reported in the literature to date have involved two-photon-induced polymerization. By irradiating a liquid resin with pulsed laser light, the exposed region is converted into solid structures. The light source normally is a femtosecond near-IR laser beam, which induces two-photon absorption leading photopolymerization within the resin. As in conventional lithographic methods, the unreacted liquid resin is then removed. Arbitrary 3D structures can be fabricated by this method.

Two-photon methods can be used to produce patterns of remarkably high resolution in 3D. By far, various micro-devices[12,13] and photonic crystals[14,15] have been readily produced by this method with high resolution. In one such study, the diffraction limit was exceeded due to the nonlinear effects and a spatial resolution of 120 nm was obtained using 780 nm light[16]. Fabrication of 3D "microbull" sculptures and a functional micro-oscillator (a spring) system were demonstrated in this study. The bull sculptures, 10 μm long and 7 μm high, were the smallest animal models produced to date and were about the size of a red blood cell. Therefore, this method has the potential use for fabricating microcapsule-based drug delivery systems. At the same time, the micro-oscillator system was also acclaimed to be the smallest functional micromechanical system produced to date, having a spring diameter of 300 nm.

Two-photon polymerization methods are also applicable in biomedical areas. One of the most promising approaches is in tissue engineering, where the technique is being used to prepare scaffolds for guided and controlled 3D tissue growth. In one study[17], the biocompatible organic-inorganic hybrid polymer -- ORMOCOMP-- has been used for the fabrication of such scaffolds. It was shown that different cell types grew on the vertical surfaces of 3D structures composed of ORMOCOMP.

To sum up, photoresist-based polymerization methods are the most common methods employed with two photon process as demonstrated above. Desired 3D structures are fabricated by laser-induced photopolymerization and subsequent removal of the unreacted liquid resin. This two-photon 3D lithography could become a useful and powerful technique in future micro- and nanotechnology.

1.1.3 Laser Ablation Based Methods

Laser ablation emerged as a lithographic method about twenty years ago. It is a process of removing material from a solid (or occasionally liquid) surface by irradiating with a laser beam. At low laser flux, the material is heated by the absorbed laser energy and evaporates. At high laser flux, the material is typically converted to a plasma. The depth over which the laser energy is absorbed, and thus the amount of material removed by a single laser pulse, depends on the material's optical properties and the laser wavelength.

Many applications of laser ablation have been reported so far, the simplest being the removal of material from a solid surface in a controlled fashion. Laser machining and particularly laser drilling are examples of this application. Also, laser energy can be selectively absorbed by coatings, so laser pulses can be used to clean surfaces, remove paint or other coatings, or prepare surfaces for painting without damaging the underlying substrates. Another class of applications uses laser ablation to process the material removed into new forms that are difficult, if not possible, to produce by other means. A recent example is the production of carbon nanotubes from laser ablation onto graphite blocks[18]. A variation of this type of application is to use laser ablation to create coatings by ablating the coating material from a source and letting it deposit on the surface to be coated[19]. This latter method represent a special type of physical vapor deposition. Last but not the least, laser ablation has numerous applications in biological[20-22] and aerospace[23] sciences.

1.2 Laser Ablation Lithography in Polymers

A little over twenty years ago, two groups, working independently of each other simultaneously reported that ultraviolet laser pulses of nanosecond duration were capable of etching organic polymer films without any need for further development. These reports led to a huge burst of activity from numerous groups all over the world to explore this technique. The high level of activity in this area continues even today. The driving force behind laser ablation research, as mentioned before, was and continues to be the potential of this method for applications in several areas, including optoelectronics[24], organic semiconductors[25], biological systems[20-22], and microfluidic devices[26].

The remainder of this section covers the history of the technique, mechanisms and models describing ablation, polymers investigated, light sources for ablations, and applications of ablative polymer film patterning.

1.2.1 Brief History

Laser ablation and ablative photodecomposition, which are now commonly in use, were pioneered by R. Srinivasan[27], who first reported laser ablation in 1982. Y. Kawamura[28] described similar experiments in the same year. After these initial demonstrations, many research groups worked to develop laser ablation into an industrially-relevant procedure. Today, commercial applications primarily cover two main areas: the preparation of via holes in polyimide for multichip modules[29], and the production of inkjet printer nozzles[30].

1.2.2 Ablation Mechanisms and Models

1.2.2.1 Ablation Mechanisms

The ablation process involves the removal of a solid (or occasionally liquid) material from a substrate surface by laser irradiation at a specific power. At low fluence, the material is heated by the absorbed laser energy and evaporates. When the fluence is above the threshold, the ablation rate increases. The etching threshold depends on the material properties and laser wavelength. Pulsed lasers are most often employed for laser ablation. Laser pulse durations can range from nanosecond to femtosecond. In all cases, flux must be precisely controlled.

The actual mechanisms involved in ablation processes have been argued for decades. It is now generally believed that the energy from the laser pulses first leads to electronic excitation of the polymer. The subsequent conversion of this energy to a useful form (for ablation) could occur by several different mechanisms.

Two dominant mechanisms responsible for the onset of ablation involve photothermal[31] and photochemical[32] processes. Photochemical processes lead to electronic rupture of chemical bonds in the molecule, while photothermal processes heat the sample to the point at which it decomposes. It is generally believed for lasers operating at visible or infrared wavelengths, that photothermal processes are dominant, while with the far-UV laser irradiation, when the photon energy is larger than the energy of the chemical bonds in the molecule, photochemical processes are dominant for the onset of ablation.

1.2.2.2 Models for Ablation

Researchers have reported several different models for ablation. A few of these will be described here.

The first model to be explored employs the simple but constructive idea that polymers consist of long molecular chains, incorporating strong, covalent bonds within individual chains. At the same time, it is assumed different chains interact with each other very weakly. Upon irradiation by UV light, the covalent bonds will break up, leading to "depolymerization" of the polymer. Taking into account the Bouguer-Lambert-Beer intensity distribution inside the material, an easy "photochemical law"[33] can be described as below:

$$h_e = \begin{cases} 0, & \text{if} \Phi < \Phi_{th} \\ \frac{1}{\alpha} \log\left[\frac{\Phi}{\Phi_{th}}\right], & \text{if} \Phi \geq \Phi_{th} \end{cases}$$

Where h_e is the etch depth (per pulse), α is the absorption coefficient (absorbance of a sample at the laser wavelength is a key factor since the first step of ablation is absorption of photon energy), Φ is the laser fluence, and Φ_{th} is the threshold fluence.

The second model is a photothermal model, in which case the absorbed laser energy increases the temperature until the polymer is thermally decomposed. In this process, the chain breaking that occurs with ablation is governed by Arrhenius Law, but thermal diffusion in the polymer and its heat capacity also need to be taken into consideration.

1.2.3 Materials

Two major classes of polymers have been studied for use with laser ablation methods. They include neat polymers and doped polymers. Neat polymers are ablated by direct interactions of the polymer itself with light, while doped polymers have specific dopants added to them. These dopants act to absorb the incident laser light and to serve as sensitizers of the polymer to be ablated.

1.2.3.1 Neat Polymers

The ablation of pure polymers may be usefully treated in terms of the ablation of existing commercial polymers and the ablation of polymers especially designate to yield desirable ablation behavior. The design of polymers to maximize ablation rates and quality was recently review[34].

1.2.3.1.1 Commercial Polymers

Polyimide (Kapton), poly-methyl methacrylate (PMMA), polyethylenterephthalate (PET) and various fluoropolymers such as Teflon (PTFE) have been intensively investigated. Only the first two will be discussed here. Figure 1.2 shows chemical structures for Kapton and PMMA[35].

Kapton is the most well studied commercial polymer so far, mainly because it can be ablated with all common excimer lasers and pulse lengths. Kapton also has wide applications in many technical fields. Perhaps its most common use is as a dielectric in microelectronics for multichip modules[36]. Kapton characteristically carbonizes during laser ablation, a fact that can be exploited to produce conducting surface layers. The decomposition mechanism had been investigated by several time-resolved techniques, such as shadowgraphy[37], interferometry[38] and reflectivity[39]. According to nanosecond shadowgraphy[37], all the excimer wavelengths yield similar blast waves, however, the nature of the ejected materials should depend strongly on laser wavelength. At 248 nm, only a weak trace of opaque material is visible in shadowgraphs, but at 308 nm and 9.17 μm, an obvious increase solid material was shown. At the same time, interferometry spectra[38] at 248 nm showed material removal from Kapton was confined to the duration of the laser pulse and yielded no solid debris. At 351 nm, clear surface swelling was observed, followed by the ejection of solid particles and prolonged material removal. These observations indicate the ablation mechanism changed from photochemical (248 nm) to photothermal (351 nm).

Decomposition products of Kapton ablation have been studied by diffuse reflectance infrared fourier transform spectroscopy (DRIFTS) after irradiation at 308 nm[40]. Possible mechanisms for laser-induced decomposition[40] and thermal decomposition[41] are illustrated in Figure 1.3 and 1.4. Initial bond breaking happens at two places, the phenol-O and the N-C bond in the photochemical mechanism (Figure 1.3), while thermal processes decompose the polymer mainly at the N-C bond (Figure 1.4). Both cases produce bulk carbon deposits on the substrate surface.

Another polymer that has been widely investigated for laser ablation applications is PMMA. PMMA is normally etched with wavelengths shorter than 308 nm. At 308 nm, ablation quality is poor because of the low absorption coefficient since its absorption maximum is 213

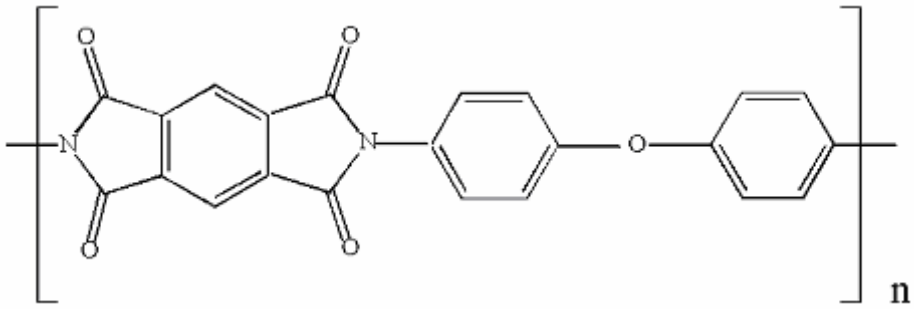

Polyimide (Kapton)

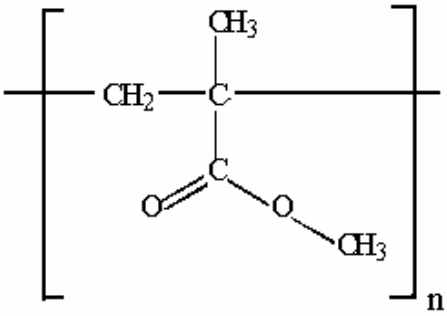

Polymethyl-methacrylate (PMMA)

Figure 1.2 Chemical structures of PI (Kapton) and PMMA. Modified from ref 35.

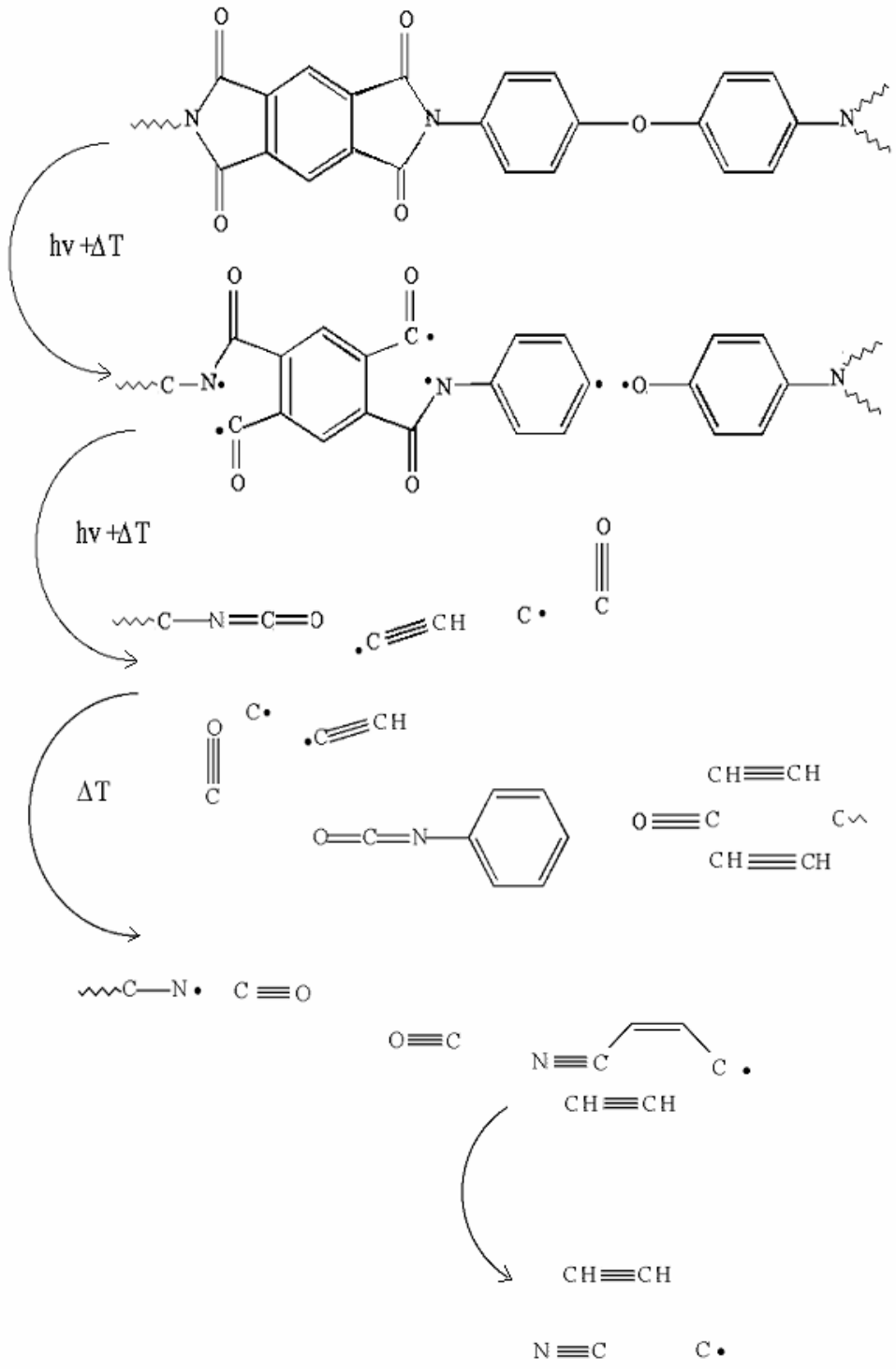

Figure 1.3 Suggested decomposition schemes for photochemical ablation of Kapton. Modified from ref 40.

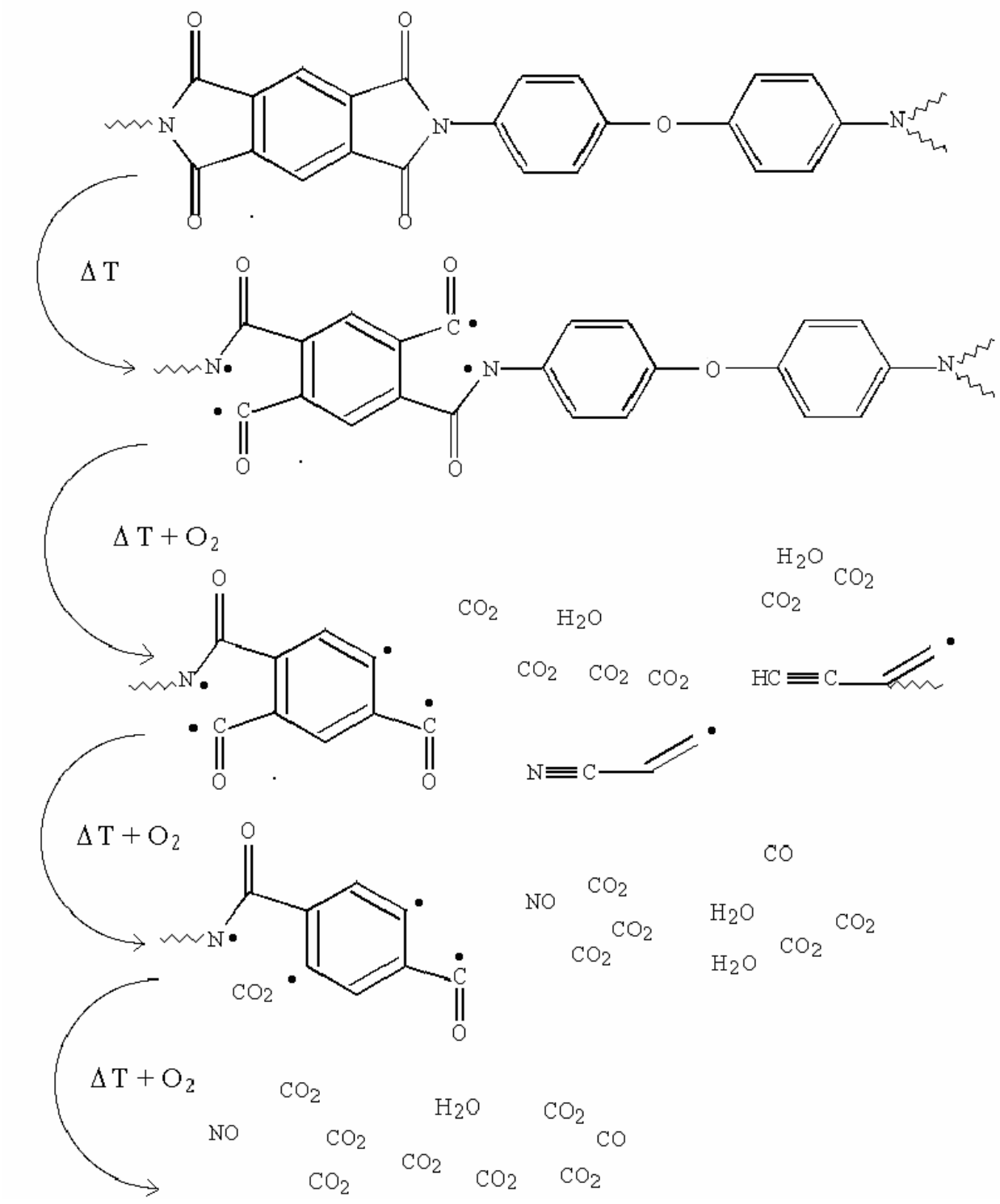

Figure 1.4 Suggested decomposition schemes for photothermal ablation of Kapton. Modified from ref 41

nm[42], but at 248, 222, 216 and 193 nm, etching produces good structures. Yet, it is believed direct ablation only occurs at 193 nm. At all other ablation wavelengths, it has been proposed that "incubation" must happen first. Stuke[43] and Srinivason[44] demonstrate that during incubation, the chemical structure of the polymer changes, which raises its absorption coefficient at the laser wavelength. Subsequent absorption then causes ablation. Photochemical reactions create defects which serve as absorption sites, allowing for ablation to occur at even longer wavelength after incubation.

A possible decomposition scheme for PMMA ablation is given in Figure 1.5, based on TOF-MS analysis[45]. The first three steps are related to incubation, while step 4 is depolymerization in which the polymer chain fragments are broken into monomer units.

1.2.3.1.2 Modified Commercial Polymers

The ablation properties of polyestercarbonates (PEC, structure shown in Figure 1.6) have also been studied[46]. In these studies, etching behavior has been shown to change with chemical modification of the polymer. When l=0, in which case the polymer is an aromatic polycarbonate (containing OCOO groups), the absorbance maximum is at 308 nm, and so etching can be accomplished with an excimer laser operating at 308 nm although the fluence has to be as high as 2 J cm^{-2} to surpass the etching threshold (see Figure 1.7a). However, the quality of ablation was found to be poor. The edges were not sharp, the etched area was not smooth, and a lot of debris was produced. In contrast, by adding 30% molar fraction of the ester into the polymer, much better etching behavior was obtained, as evidenced by SEM images of etched structures (see Figure 1.7b). The substitution of aromatic ester groups to the polymer increases the absorbance and ablation rate and also decreases the fluence threshold.

It is possible that the products of gaseous decomposition, which would be CO and/or CO_2, could carry away a lot of ablation fragments, and as a result, a polished surface is formed as in Figure 1.7 (b).

1.2.3.2 Doped Polymers

Ablation processes for doped polymers depend largely on the absorption properties of the polymer-dopant system. These systems range from polymer blends, to systems where only the dopant or only the polymer absorbing. Therefore, ablation results from a complex mixture of

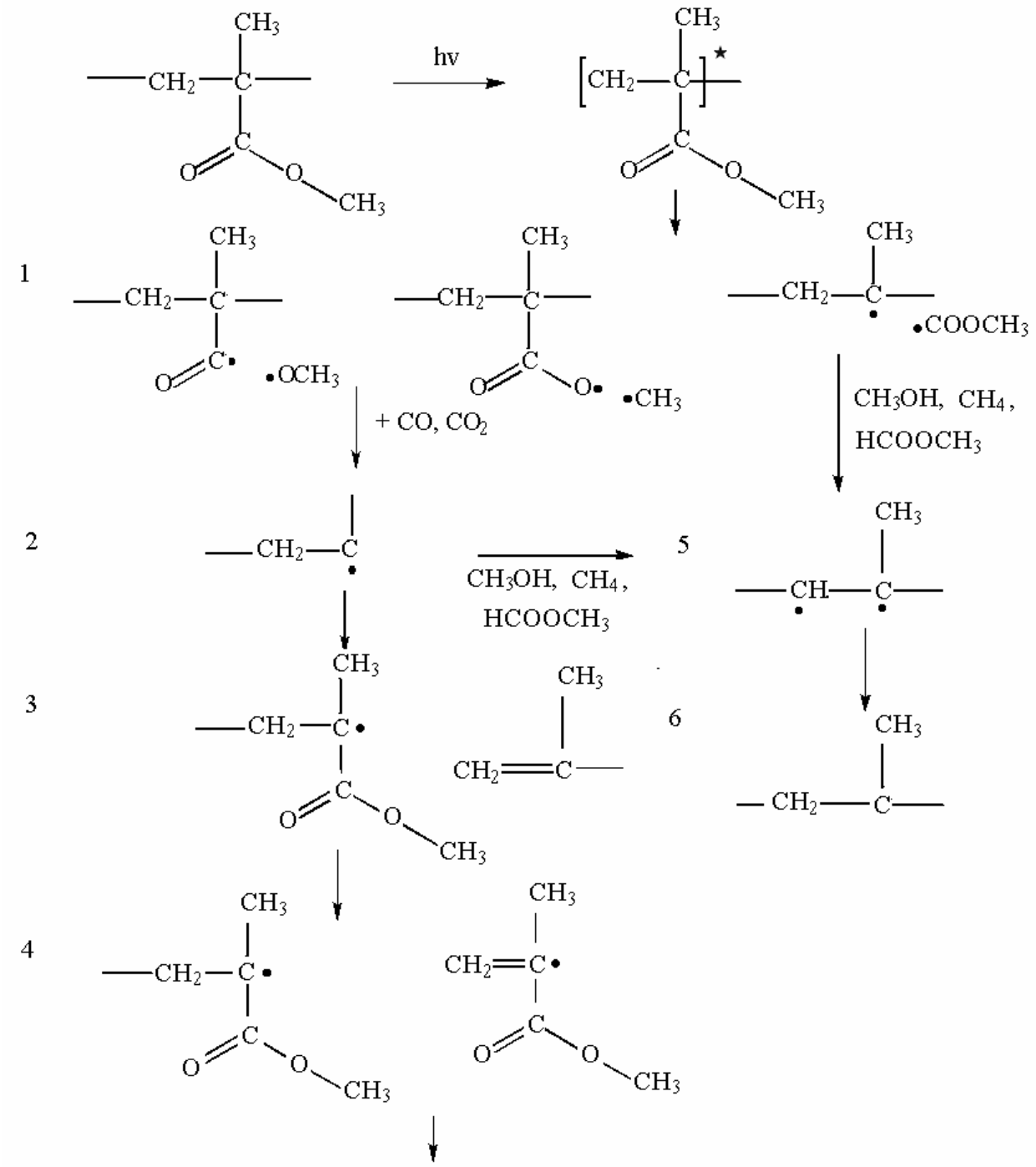

Figure 1.5 Possible incubation and decomposition scheme for PMMA etching at 308 nm. Step I and II show the photolysis of the ester side chain, the typical small produces detected in mass spectrometry measurements, and the double bonds that are created during incubation. Step IV show the photochemical and thermal activated reaction to release MMA. Modified from ref 35.

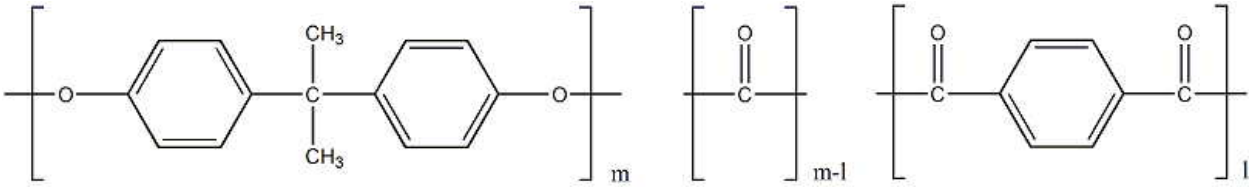

Figure 1.6 Chemical structures of PC (l=0) and PEC with certain amount of ester content. Modified from ref 35.

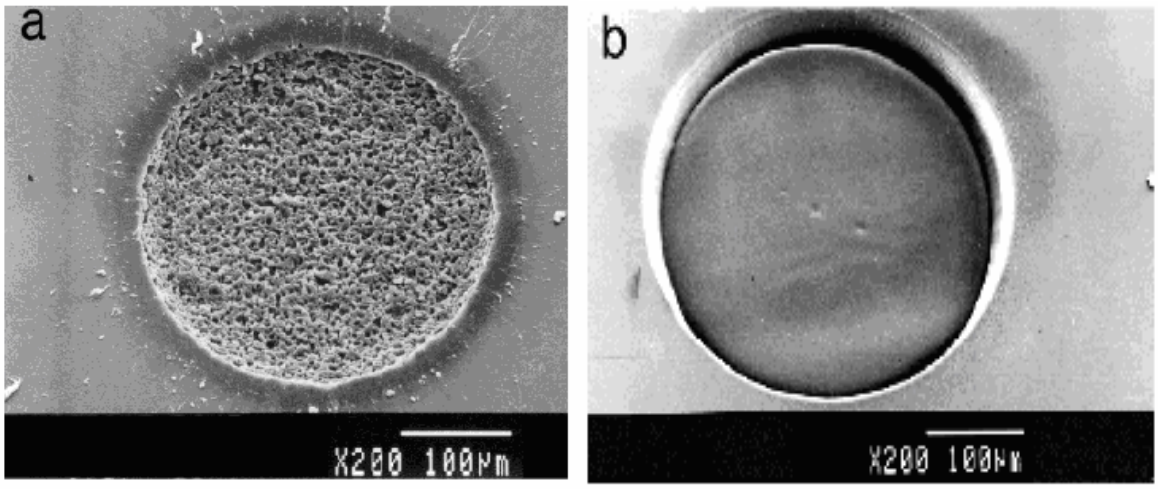

Figure 1.7 SEM images for etching of (a) PC, irradiation at 308 nm with 15 pulses and a fluence of 7.66 J cm^{-2}. (b) PEC, with 30% molar ratio of ester groups, irradiation at 308 nm, 15 pulses and a fluence of 18.45 J cm^{-2}. Reprinted with permission from ref 35.

processes originating from the dopants or the matrix. Depending on the properties of the dopant, different ablation pathways are dominant.

The ablation behavior of doped polymer systems with absorbing dopants depends strongly on whether absorption actually decomposes the dopant molecule. Photolabile dopants that decompose to gaseous products typically produce pronounced surface swelling at low fluences (shown in Figure 1.8 a). Very high ablation rates (up to 80 μm per pulse) can be achieved at high fluence[47], but always with pronounced signs of surface melting (Figure 1.8 b). In contrast, photostable dopants (e.g., polyaromatic compounds) produce much less surface swelling and lower ablation rates.

Dopants can be employed as probes of the ablation process for polymers in general. However, one must account for dopant-induced changes in the polymer properties (e.g., depression of the glass transition temperature). One must also distinguish the role of dopant as a molecular probe from potential active involvement in the ablation mechanism. Dopant-induced ablation is a real possibility with behavior often sharply contrasting with the neat polymer (e.g., wavelength dependence). Once properly accounted for all these influences, doped polymers are an important tool to elucidate the role of polymer chemistry in polymer ablation. The wide range of behaviors that have been demonstrated with various dopants offer many possibilities for practical applications. For instance, carefully chosen dopants allow for structuring of "unprocessable" polymers (PTFE)[48] or structuring at longer wavelengths[49].

1.2.4 Light Sources for Ablation

1.2.4.1 Low Intensity (Lamp) Sources

Lasers are capable of modifying the surface structures of polymers, but the high cost of many laser sources restrains their commercial applications. However, lasers are still used under many circumstances, such as when very high spatial resolution is required and the area to be patterned is small. They are also useful when arbitrary patterns are to be produced. In most lithographic methods, low intensity UV and VUV lamps are employed. These lamps include mercury lamps outputting at 185 nm, Xe resonance lamps at 147 nm[50], helium discharge lamps with $\lambda < 160$ nm[51], and excimer lamps at 146 (Kr_2)[52], 172 (Xe_2)[53], 222 (KrCl)[54], and 308 (XeCl)[55]. Under well controlled conditions, even polymer etching has been achieved with mercury lamps and excimer lamps.

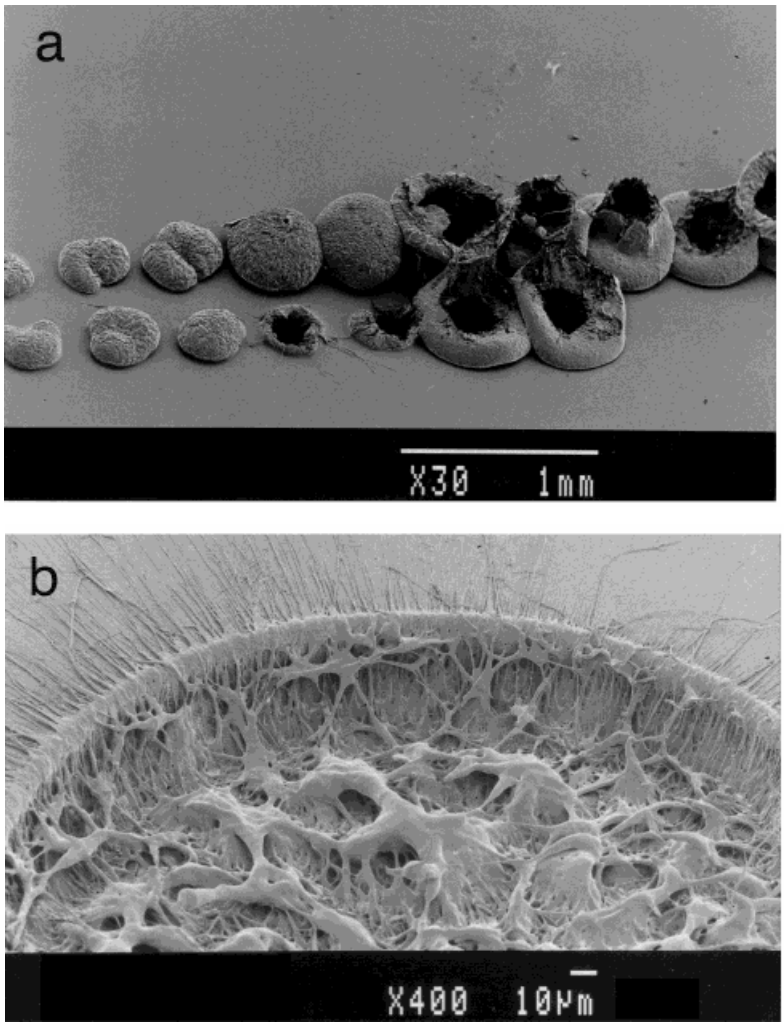

Figure 1.8 (a) Surface swelling and bubble formation during ablation of PMMA doped with low dopant concentration (0.25 wt% of a dialkyl-aryl triazene-compund). Irradiation at 308 nm with single pulses and increasing fluences (from left to right). (b) PMMA doped with 2 wt% of the dopant and irradiated with 2 pulses of 5.8 J cm^{-2}. Reprinted with permission from ref 35.

1.2.4.2 Continuous-Wave UV Lasers

CW UV lasers have been used to etch polymers such as PMMA[56]. Ar-ion lasers operating at 351, 363, 300-330, or 350-380 nm have been employed in many situations. In studies of neat PMMA etching, Ar-ion lasers emitting CW radiation at 351 and 363 nm were used to expose onto the polymer, producing an effect similar to incubation[57]. Structuring polymers with these CW laser is very different from excimer lasers since etching by CW lasers most likely occurs by a photothermal mechanism.

1.2.4.3 Femtosecond Lasers

IR solid state (Ti:sapphire) lasers have become compact, extremely high-intensity sources, especially with the development of chirped pulse amplification[58]. Several characteristic advantages are associated with ablation caused by femtosecond lasers. These include the production of a negligible heat-affected zone, a lower ablation threshold, absence of plasma shielding, and the capability to structure "transparent" materials.

Several publications have shown that ablation methods employing femtosecond lasers can produce higher quality structures. In contrast, nanosecond lasers operating at the same wavelength only damage the surface. It has also been shown that the ablation threshold is lower for femtosecond lasers when compared to nanosecond systems. Srinivasan's original experiment[59] on PMMA clearly showed that at 308 nm, 160 fs pulses produce high resolution structures, while nanosecond pulses simply ruin the surface. Stuke[60] ablated PMMA with 300 fs, 248 nm laser pulses, and showed this method had a threshold five times lower than when a ns laser was employed. For Teflon, no evidence of thermal degradation was found with femtosecond laser pulses, and very high quality structures could be produced[61]. Time-resolved studies[62] employing a pair of time-delayed 500 fs pulses at 248 nm show the ablation rate depends upon the time delay, especially when the combined fluence is close to the threshold. Very significant changes could be observed for PMMA and Teflon for delays smaller than 3 ps. Therefore, it is reasonable to state that multiphoton absorption dominates the ablation process for those two polymers.

Ultrafast laser ablation methods are still very new and many questions remain unanswered. Perhaps most importantly, the exact mechanisms for ablation remain uncertain. Incubation steps are often thought to be involved in ablation processes, yet the chemical/physical changes that occur during incubation are not fully understood. Nevertheless, femtosecond

ablation methods clearly have the potential for patterning a wide variety of polymers with very high resolution and minimal heat affected zone.

1.2.4.4 Vacuum-Ultraviolet (VUV) Lasers

VUV lasers are an important alternative to femtosecond lasers for polymer ablation. Very short wavelengths can be achieved with VUV lasers which could produce smaller and finer structures. The high photon energies (e.g., 7.9 eV at 157 nm) can easily break chemical bonds and drives photochemical ablations under most circumstances. But VUV ablation needs to be performed under vacuum, or at least under inert gases. Furthermore, because short wavelengths are employed, expensive optical elements are often required. Still, VUV is an attractive alternative because of higher resolution. And VUV excimer laser beams are relatively large with flat-topped intensity profiles compared to Gaussian beams from Ti:sapphire lasers. This helps pattern large areas in a short time.

1.2.5 Applications to Polymers

Laser ablation methods are applicable in a wide variety of fields, including modification of biological tissues[63,64], laser cleaning of painted artwork[65], polymer films deposition[66,67], matrix assisted laser desorption ionization (MALDI Mass Spectrometry) and related techniques[68-71], and ablation of molecular solids and liquids[72].

One study[73] claimed it is possible to remove the fiber jacket for side written gratings by laser ablation. Fiber Bragg gratings (FBG) are an important class of components developed in the telecommunication field. For side written gratings, although it has been demonstrated in some cases that the polymer jacket is sufficiently transparent for transport of a high enough irradiance to the core/cladding interface, it is usually necessary to remove the outer layer of the fiber. In this reference, possible ways for removing this fiber jacket have been analyzed. Other than common means, like mechanical stripping which causes structural damages to the fiber, or chemical stripping, in which the chemicals used are volatile and environmentally undesirable, laser radiation overcomes all the limitations listed above. The KrF excimer laser has been shown to offer the most efficient removal rate, with a lower fluence. SEM micrograph of a fiber jacket, stripped from one side by translating the target through a line focus orientated perpendicular to the irradiation, showed that KrF excimer laser is suitable for fiber jacket stripping with minimum possible damage to the silica fiber.

In another study[74], direct-write laser ablation from a KrF excimer laser with a circular beam was employed to fabricate microlenses in polycarbonate materials. The beam was obtained by imaging a circular aperture onto the polymer surfaces. Scanning is realized by the translation stage carrying the sample, leading to fabricate successive contours in the film, when well-chosen beam diameters and scan velocities are employed. A dedicated software tool calculates the exact path and positions of overlapping circles, which are required to obtain a desired lens shape. Afterward, a large beam aperture covering the full lens area is used to ablate the lens deeper into the substrate in order to smooth the ablated surface and release it from debris. Spherical lenses with a broad range of f-numbers have been fabricated.

Ultra-thin films of poly(dimethylsiloxane) (PDMS) can also be patterned by laser ablation. It has been pointed out that PDMS forms a strong chemical bond with many base materials and its surface is rather chemically inert[75]. The effect called LIAD (light-induced atom desorption)[76] has been found in PDMS, which can store highly reactive alkali metals and release them via illumination with low-power light and store them again. Since LIAD turns PDMS film into an optically switchable source of clean alkali metals and since it is usable under ultra-high-vacuum conditions, it is an ideal reservoir for atomic optical experiments. It was suggested that to prepare square-like structures in PDMS films, where these features could serve as micron-scaled reservoirs for foreign atoms. In reference 74, such structures were fabricated by 193 nm pulses, with square height at 8 nm and width at 2 μm. It is important that ablation in this case is not accompanied by modification of the remaining surface. Micro-Raman measurements indicate no radiation induced reactions in the remaining polymer film. So, laser ablation is a useful technique to produce desirable structures in PDMS films.

Ultra-short pulsed near-IR lasers have also been used to realize laser ablation. One study[77] demonstrated a SEM image of a 500-μm motor machined into bulk poly(tetrafluoroethlene) (PTFE) sample using a 800-nm femtosecond Ti:sapphire laser. At femtosecond pulse durations, the absorption of laser light by PTFE is enhanced through a multiphoton absorption mechanism. Precise holes and channels free from collateral thermal damage could be generated.

Another study investigated femtosecond pulse laser damage on poly(3,4-ethylene dioxythiophene)-poly(styrenesulfonate) (PEDOT-PSS) films of varying thickness on Au/Pd substrates[78]. Damage produced by a single laser pulse in PEDOT:PSS films of varying

thicknesses was explored. For two films (thicknesses at 62±6 nm, 297±18 nm), the gold/palladium substrates were exposed after only one pulse, while in the other two films (thicknesses at 608±21 nm, 1900±120), the substrates were not visible, but the PEDOT:PSS films appeared darker than non-irradiated areas. FTIR spectra of the unmodified film and film areas irradiated above were also collected. These spectra showed almost no difference, therefore it is reasonable to believe the darker color of the irradiated areas is caused by changes in the physical property rather than chemical properties of the films.

Other than single shot damage, linear trenches have also been prepared in PEDOT:PSS films. These trenches were ablated by laser fluences which were close to the damage threshold for all PEDOT:PSS film thicknesses. AFM images of the line features prepared in films of four different thicknesses showed that the depths of the lines corresponded approximately to the thickness of the film. The trench depths did not increase with higher fluences, indicating that the films were completely removed under these conditions.

1.3 Summary

Laser ablation of polymers is a valuable technique with applications in micro- and nano-electrochemical systems[79] (MEMS, NEMS), microfluidic devices[26], photonic crystals[80], 3D optical data storage[81], tissue engineering scaffolds[17], and drug-deliver devices[82]. Debates on ablation mechanisms, studies on ablated polymers, and development of new ablation tools are ongoing and will continue into the foreseeable future. A number of exciting improvements and more applications of laser ablation has been seen in the past decades. Among all the new techniques, femtosecond lasers are particularly expected to lead to new industrial applications.

1.4 Overview of Thesis

In chapter 2, the experimental details associated with the binary and grayscale patterning of PEDOT:PSS films are presented. In chapter 3, experimental results will thoroughly be discussed, and conclusions concerned with PEDOT:PSS etching will be drawn based on scientific analysis. At last, Chapter 4 will conclude this entire study and debate the future work.

CHAPTER 2 - Experimental Methods

In this chapter, the experimental procedures specific to the studies described in this thesis will be discussed thoroughly. The three main topics covered are 1) preparation of PEDOT:PSS films, 2) multiphoton lithography and 3) AFM imaging and data analysis.

General aspects are discussed in this chapter. Parameters and detailed methods associated with specific experiments are described with those experiments in chapter 3.

2.1 Preparation of PEDOT:PSS Films

Optical clear materials which possess electrical conductivity are sought for the fabrication of flat panel displays and other electronic devices. Poly(3,4-ethylenedioxythiophene), commonly known as PEDOT, has excellent transparency in the visible region, good electrical conductivity, and good environmental stability, all of which make it extremely attractive for organic electronics applications. It has already been utilized in a wide variety of organic-based optoelectronic devices[83]. It has also been used as a charge injecting layer in light emitting devices[84], as a component in electronic displays[85], and as electrodes in field effect transistors[86] and photovoltaic cells[87]. Unfortunately, by itself, PEDOT, like most conducting polymers, is infusible and insoluble and therefore is difficult to process in a thin-film form or in other shapes. This lack of processability has been the main obstacle to the commercial acceptance of this polymer.

PEDOT:PSS – poly(3,4-ethylenedioxythiophene)poly(styrenesulfonate), commercially known as Baytron® P, is a conducting polymer mixture of two ionomers (shown in Figure 2.1 a). One outstanding property of this complex is its water "solubility". It was developed by Bayer AG Co. and commercially available in a number of grades from H.C.Starck (a Bayer subsidiary) as a dispersion in water (typically at 1-3 % wt. solids) (shown in Figure 2.1 b). It has been observed that the deposition of a thin film of PEDOT:PSS on ITO electrode surfaces increases the maximum luminance of organic light emitting diode (OLED) devices up to three orders of magnitudes, reduces the threshold voltage by more than 50%, and increases device lifetime by a factor of 10[88]. Baytron® P solution can be spin coated or inkjet printed, and devices that contain Baytron® P as the hole-injecting layer (HIL) have shown dramatically improved brightness,

(a)

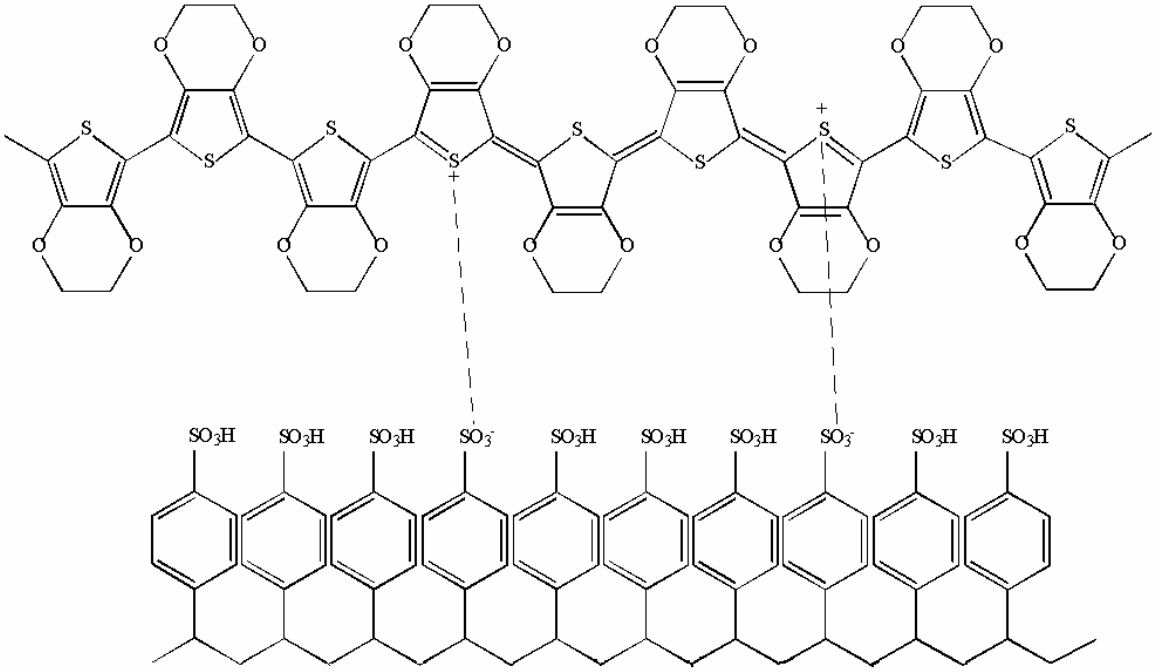

(b)

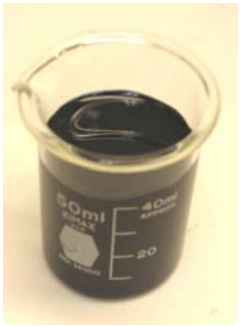

Figure 2.1 Scheme of PEDOT:PSS (a) and a beaker of Baytron® P (b).

lower driving voltages, and fewer malfunctions[89]. Nevertheless, Baytron® P does have some drawbacks. Since the dispersion is very acidic due to the high loading of PSS in its acidic form, this causes problems during application. For example, PEDOT:PSS does not wet organic substrates without a high loading of binders or complex formulation, both of which decrease the conductivity of the resulting film[90]. Moreover, many electronic applications cannot tolerate the presence of water.

The Baytron® P used in this thesis is from H.C.Stark, provided as a free sample. The weight percentage ratio between PEDOT and PSS is 1:2.5. The whole weight percentage is 1.3%. In order to increase wettability onto substrates, the PEDOT:PSS solution was modified by adding 1 part Methanol to 3 parts PEDOT:PSS solution.

The preparation of the films starts with cleaning coverslips using a plasma cleaner (Harrick Plasma, PDC-32G). All films were spin coated onto cover glasses (Fisher Premium Cover Glasses, size of 25 x 25 mm) which had previously been cleaned at high RF. The spin coating conditions were: acceleration rate set to minimum, speed set to 2000 RPM, time period set to 30 seconds. After spin casting the solution, a thin layer film is formed on top of the coverslip, and by putting the coverslip right away into a Furnace (purchased from Barnstead Thermolyne) and baking it at 110°C for 20 minutes to dry. Films are either used directly or stored into dessicators after baking.

2.2 Multiphoton Lithography Setup

The polymer coated coverslip is loaded onto a piezoelectric scanning stage mounted on an inverted epi-illumination microscope. The laser source is pulsed near IR laser, and it will be described first, followed by microscope.

2.2.1 Titanium-Sapphire Laser System

The light source used for etching is a mode-locked Ti:sapphire laser yielding 170 femtosecond pulses of light centered at 870 nm. Therefore background information about Ti:sapphire laser is introduced first.

Ti:sapphire lasers emit near-infrared light, tunable in the range from 650 to 1100 nm with very short pulses when mode-locked. Titanium-sapphire refers to the lasing medium. A crystal of sapphire (Al_2O_3) is doped with titanium ions which makes it a transition-metal-doped gain medium. Ti:sapphire lasers are also used in continuous-wave mode with a wide wavelength

tuning range. Ultrashort pulses from Ti:sapphire lasers can be generated with mode-locking, and pulse duration around 100 fs are easily achieved and are typical for commercial devices. However much shorter pulses could be produced, some research laboratories have achieved pulse durations around 5.5 fs[91]. Common output powers of mode-locked Ti:sapphire lasers are of the order of 0.3 W to 1.0 W, and a typical pulse repetition rate is 80 MHz.

2.2.2 Microscope Setup

A diagram of the microscope used for direct-write multiphoton lithography employed in this thesis is shown in Figure 2.2[92]. For etching, a PEDOT:PSS coated coverslip is loaded onto the piezoelectric stage. The piezo stage is attached to an inverted epi-illumination microscope. Light from the Ti:sapphire laser (described above) passed through several polarization optics to control incident power, and an electronic shutter for controlling the etching process. Then, the laser light is reflected by a dichroic beam splitter into the back aperture of a 100 x, 1.3 NA (numerical aperture) oil-immersion objective. Etching behavior is determined by a pattern (patterns in form of raw data file, 8 bit unsigned pattern) fed into the microscope control software (written in house), which can produce arbitrary structures in the polymer film. Several parameters can be changed in this software, such as how large an area is to be etched, the scan rate of the sample and the pixel time. Incident powers are measured with a power meter outside of the microscope, right before the light goes into the dichroic beam splitter, and powers varied from 0.5 to 40 mW.

The setup and etching process described so far are similar to what has been reported in the literature[92]. To improve etching and to allow for better control, two significant extensions to these methods were employed in the studies presented here. One is that an accurate Z-piezoelectric stage produced by PI (Physik Instrument) is utilized, and by controlling the Z-stage, it is possible to change the focus position both manually and automatically during etching. With this improvement, a specific focus position could be reached for each etching pattern, and more importantly gray scale patterns can be produced in the polymer film. The other extension is by collecting the fluorescence data as a function of focus position, the exact focus position can be determined from the fluorescence peak. In all experiments done before, the focus position was determined manually by eye. The utilization of automated focus procedures, using multiphoton

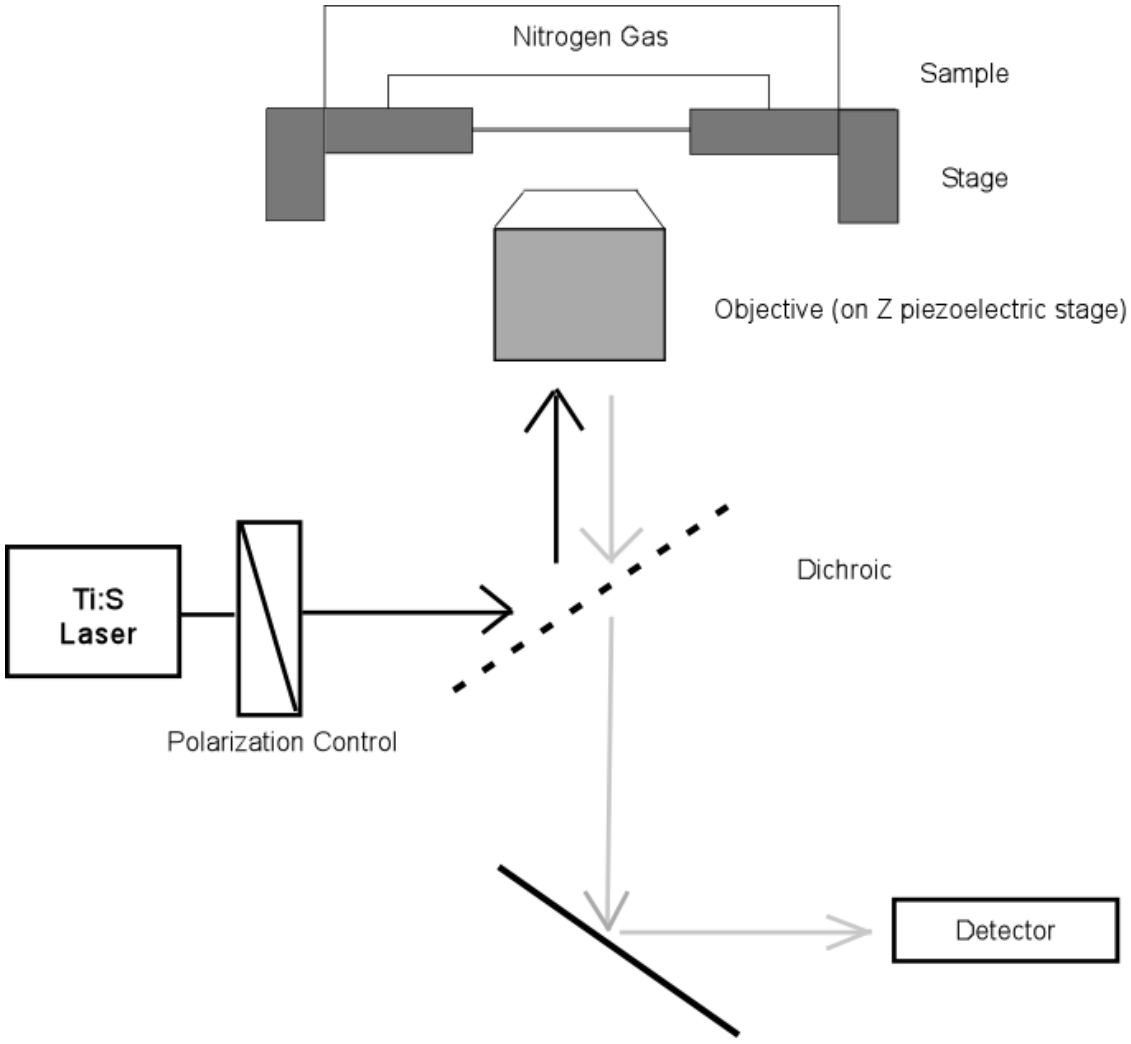

Figure 2.2 Diagram of direct-write multiphoton lithography setup. Modified from ref 92.

excited fluorescence has greatly improved the reproducibility of etching results and allows for gray scale etching to be performed.

2.3 AFM Imaging and Data Analysis

Detailed characterization of the etched samples was performed by contact-mode atomic force microscope (CM-AFM) in air. A Digital Instruments Multimode AFM with Nanoscope IIIa electronics were employed. Contact mode pyramidal AFM tips were Veeco Nano Probe^{TM} Tips (part # NP-1).

Data analysis software was programmed in Labview. This in house program loads raw AFM images properly, and allows for detailed depth information to be obtained. The software provides the average "background" height (i.e. height of unetched regions) and background standard deviation (equivalent to the RMS roughness), along with the depth and RMS roughness of user-selected etched regions. For proper depth determinations, the AFM images must be carefully leveled. During leveling, the etched regions were specifically excluded from the leveling process.

CHAPTER 3 - Results and Discussion

In this chapter, all the results obtained from laser ablation studies of PEDOT:PSS and PSS films will be thoroughly discussed. Conclusions are drawn based on scientific analysis, although some of the problems are still left open to be debated.

Prior to presenting the studies performed for this thesis, previous related studies from our group will first be described. Followed by how to use multiphoton fluorescence to determine the etching focus, under which condition most of the experiments in this thesis are accomplished. Then, binary etching of PEDOT:PSS and PSS films will be introduced, when power dependent studies are fit into a simple kinetic model reasonably well. Then the focus dependence studies of PEDOT:PSS films follow the model almost perfectly, based upon which grayscale patterning is achieved by modulating focus position. Detailed discussions are presenting as follows.

3.1 Previous Studies of Polymer Ablative Multiphoton Lithography

Ablative multiphoton photolithography has been used to prepare high-resolution two-dimensional structures in a variety of organic polymer films supported on glass substrates. Much of this work has been done by previous students in the Higgins and Ito groups. Polymers tested to date include poly(methylmethacrylate) (PMMA), poly(butylmethacrylate), poly(styrene) and a polythiophene (PTEBS)[42]. One of the main purpose of these early studies was to determine which polymers yield the best etching characteristics. PMMA was found to yield the best resolution among these polymers, exhibiting edge sharpness of ~120 nm in films of ~80 nm thickness[42], thus it was concluded that polymers possessing UV-absorbing chromophores and high glass transition temperatures produce the greatest etching resolution. A simple kinetic model for the etching process was created and utilized to fit the power dependent etching data from these polymers. PMMA was found to absorb several (4-6) photons of light at 870 nm. On the other hand, PTEBS films which exhibited the poorest etching resolution were shown to be etched by a much lower order (two-photon) process.

Although high-resolution binary structures are best prepared using materials that are etched by high order nonlinear processes, the fabrication of three-dimensional surface relief structures is hard to achieve in such polymer films because of the strong dependence of the etching rate on incident laser intensity. It was also shown in the previous studies that the film

becomes rough in partially etched regions[42]. It is expected that the three-dimensional etching will be simpler in materials that are etched by lower order nonlinear processes.

For all the reasons listed above, and because of its significant technological importance[93] in the fabrication of conducting films for use in photovoltaics[94], organic LEDs[95,96] and other organic electronic components[97], PEDOT:PSS thin films were employed in this study to fabricate grayscale (and binary) patterns by ablative multiphoton photolithography. Uniform PEDOT:PSS films of ~80 nm thickness were easily prepared by spin casting a slightly diluted (with methanol) commercially-available aqueous dispersion of the polymer onto the cover glass slides. The PTEBS polymer explored previously, in contrast, did not yield sufficient uniformity for the present studies.

3.2 Why use Fluorescence to Control Etching Focus?

As stated in the experimental methods chapter, use fluorescence to control the laser focus during etching guarantees reproducible etching behaviors. This is especially important for grayscale etching since this process requires precise positioning of the laser focus within the polymer films. Focus control was accomplished by collecting and detecting the weak blue fluorescence emitted by the films following multiphoton excitation. Figure 3.1 shows the UV-vis absorption spectrum and the one-photon-excited fluorescence spectrum obtained from dilute aqueous PEDOT:PSS solutions. The absorption spectrum is broad and devoid of resolved features in the visible and near-IR range, which is characteristic of the conducting form of PEDOT:PSS[96]. But a clear peak around 260 nm is observed and is attributed to the presence of PSS. In addition, the absorbance spectrum for a dilute PSS solution was also recorded. Again, the peak around 260 nm is due to the absorbance of PSS (Figure 3.2). Fluorescence from the PEDOT:PSS solution is peaked near 375 nm and extends well into the visible. The fluorescence spectrum shown in Figure 3.1 was excited at 210 nm and was insensitive to excitation wavelength up to at least 250 nm. Note that the blue edge of the emission spectrum is truncated by a glass slide used to block second order excitation light from reaching the detector.

Fluorescence in this same spectral range was obtained by multiphoton excitation of the polymer before film etching. Figure 3.3 plots the fluorescence obtained at low laser power (0.75 mW) as a function of focus position, which is controlled by the Z-piezoelectric stage. These fluorescence data follow the expected Lorentzian dependence on focus position[98], as

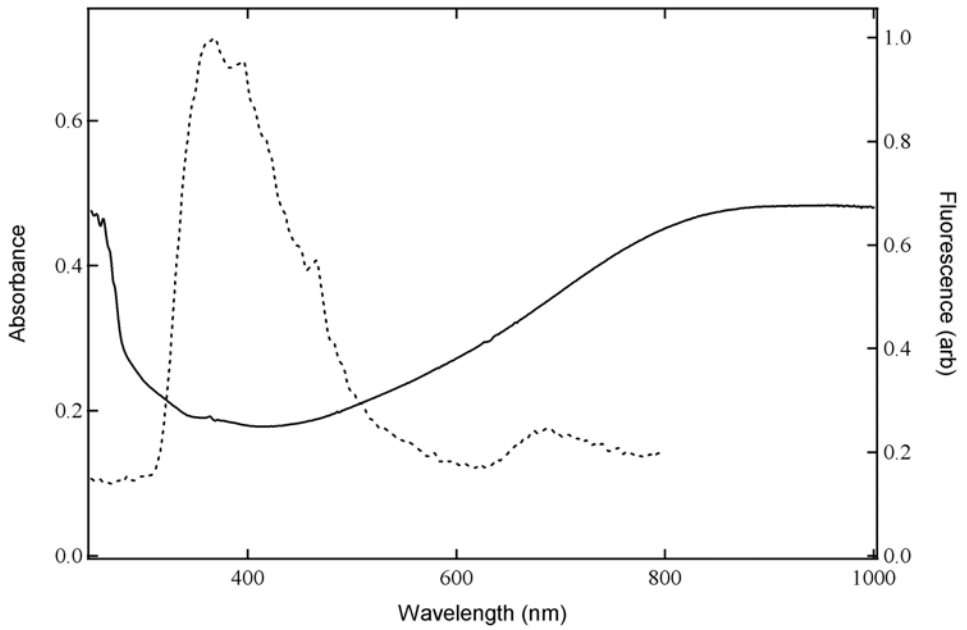

Figure 3.1 Absorbance (solid line) and fluorescence (dashed line) from a dilute aqueous PEDOT:PSS solution. The fluorescence spectrum (peaked near 400 nm) was obtained by exciting at 210 nm.

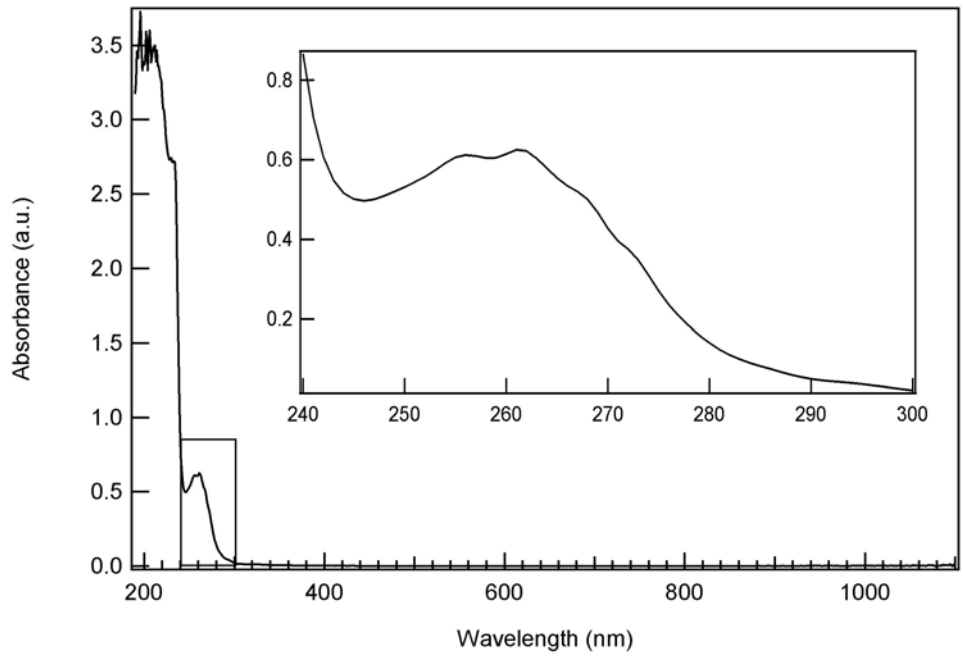

Figure 3.2 Absorbance of a dilute aqueous PSS solution. The absorbance peaked around 260 nm shows the presence of PSS (see inset for expanded view).

demonstrated by the curve fit (solid line) appended to the plot. Note that this model only applies when the polymer film is much thinner than the depth of focus of the objective lens, which is the case in this study. Maximum fluorescence is obtained with the laser focused right in the center of the film (define as 0.0 μm in the figure). However, the focus dependence of the fluorescence peak is much wider than expected, even for a linear fluorescence excitation process (plotted as a dashed line in the figure 3.3). Deviation from theory in this case is partly due to the etching and bleaching of the polymer that occurs even at very low incident powers (i.e. < 0.75 mW). Since etching and bleaching is most efficient at the focus, the fluorescence peak is somewhat suppressed, leading to broadening of the focus dependence. This broadening may also be caused by imperfections in the optical systems.

Figure 3.4 shows the fluorescence signal gradually goes down if the same spot has been scanned three times in a row at the power of 1.1 mW. However, the peak position stays the same after these scans, only the intensity decreases. This is quite important, since even if the etching and photobleaching changed the fluorescence shape, the data can still be used to determine the optimum focus position very precisely. All etching processes described in this manuscript were performed using this initial laser focus determination method.

3.3 Binary Structure Etching

3.3.1 Binary Etching of PEDOT:PSS and PSS Films

In order to properly control the ablative etching process for the fabrication of grayscale patterns, the nonlinear optical processes involved in polymer film ablation must be well understood. This was achieved by first exploring the power dependence and focus dependence of binary pattern etching in PEDOT:PSS films. Binary structures are readily constructed in PEDOT:PSS films as with other polymers we tested before[42]. Figure 3.5 shows a representative AFM image of a binary text pattern etched into one such film. This pattern was etched at 10 mW, and was 50 x 50 μm^2 in size. A line profile plot (Figure 3.6) shows that the film was completely etched away except for the text characters.

AFM images of a series of 5 x 5 μm^2 regions etched at different incident laser powers (fixed focus) are also presented below. Surface topographic data obtained from these images and

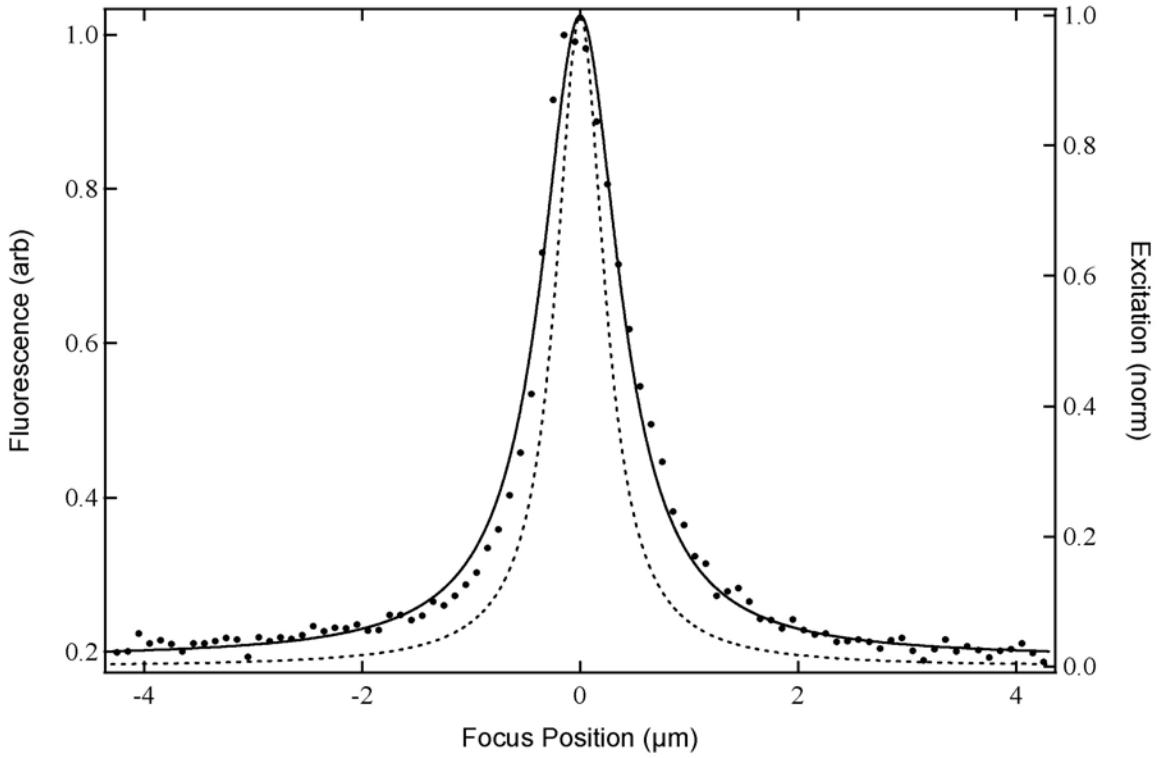

Figure 3.3 Dependence of multiphoton excited PEDOT:PSS films fluorescence on focus position. Plotted are the experimental data (squares), their fit to a Lorentzian function (solid line), and the expected profile for one photon fluorescence excitation. The experimental fit curve is broadened significantly by bleaching and etching of the polymer film.

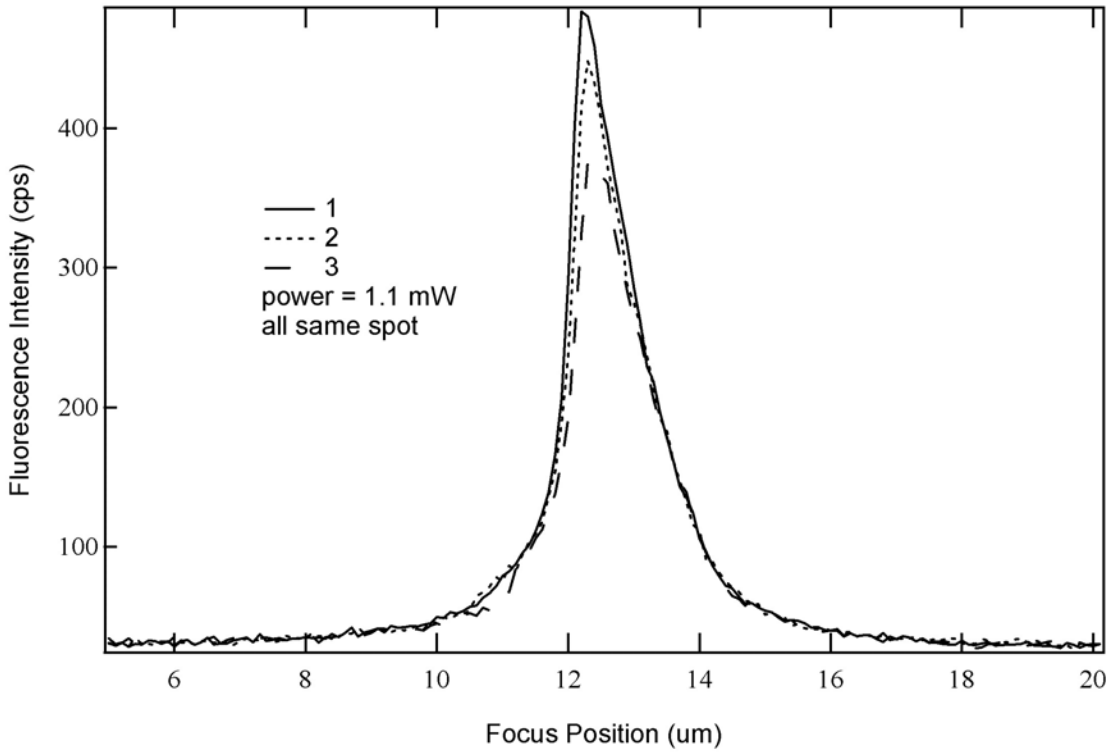

Figure 3.4 Fluorescence from the same spot after scanning three times. A significant decrease in the fluorescence signal demonstrates that photobleaching and etching after the appearance of this curve.

Figure 3.5 Binary text pattern, 50 x 50 μm^2 in size.

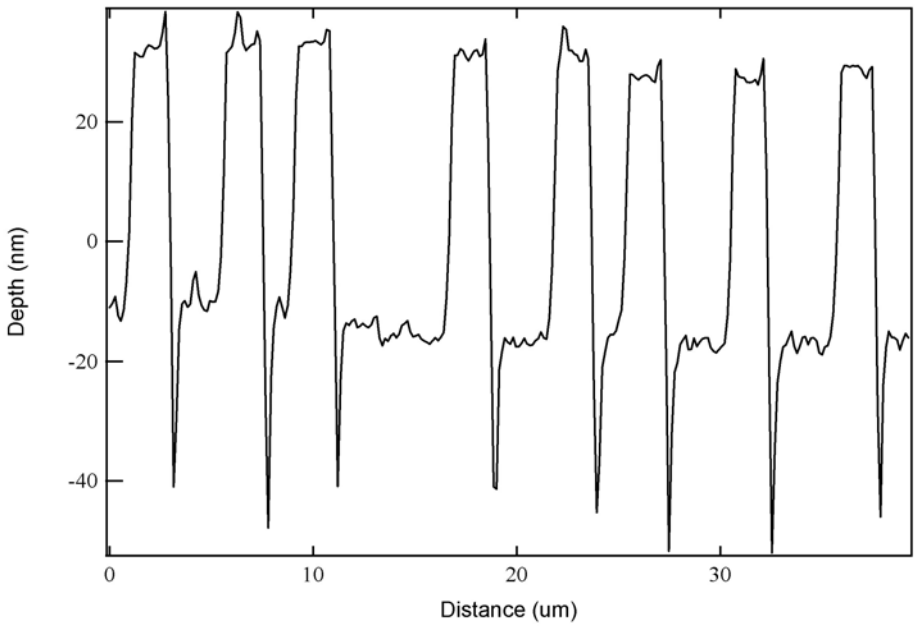

Figure 3.6 A line profile (black line in the Figure 3.5) plotted across the characters.

others like them yield an RMS roughness for unetched PEDOT:PSS of 1.0 ± 0.1 nm, indicative of the level of film uniformity achieved.

The ease by which PEDOT:PSS films can be etched is somewhat surprising. Unlike the previous polymers we have tested, all of which were single component materials[42], PEDOT:PSS is a polymer mixture, with PSS serving as the majority component (in a 1:2.5 PEDOT:PSS ratio). From our previous work[42], it might be expected that PEDOT and PSS would be etched by nonlinear processes of markedly different orders. PEDOT etching might be expected to involve one or two photon absorption, as deduced from its UV-vis-IR absorption spectrum, while PSS etching would likely require three to four photon excitation.

To determine the effective order of the nonlinear process(es) involved in PEDOT:PSS etching, the dependence of film etch depth on incident laser power was determined. In these experiments, a series of 5 x 5 μm^2 regions were etched at fixed focus using different laser powers. Figure 3.7 presents typical AFM data from such experiments, while a line profile taken across these data is also shown in Figure 3.8. The etching powers are listed on top of each etched region. Etch depths at different powers were determined by measuring the average change in film height for each etched region. Figure 3.12 (a) plots the results obtained from the data shown in Figure 3.7. It is quite obvious that etching starts at fairly low incident powers from these data, indicating that etching process is a low order process. Several replicate experiments lead to this same conclusion. At last, an AFM image was taken after scratching part of the film off to determine the full thickness of the film.

For the purpose of comparison to PEDOT:PSS films, single component PSS films were also prepared and etched in an identical fashion. In this case, a small amount of rhodamine B dye was added to the PSS spin casting solution (with an ~100 nM dye concentration). The presence of the dye allowed for the fluorescence-based focusing procedure described above to be implemented. The dye concentration employed was deemed sufficiently small to avoid interfering with the etching processes[99]. A typical AFM image of PSS etching is shown in Figure 3.11. Figure 3.12 (b) shows the power dependent etch depth results obtained from an ~90 nm thick PSS film. As is consistent with our previous results[42], etching of PSS exhibits a threshold of ~15 mW, below which no etching is observed. A steep rise is also found above this threshold.

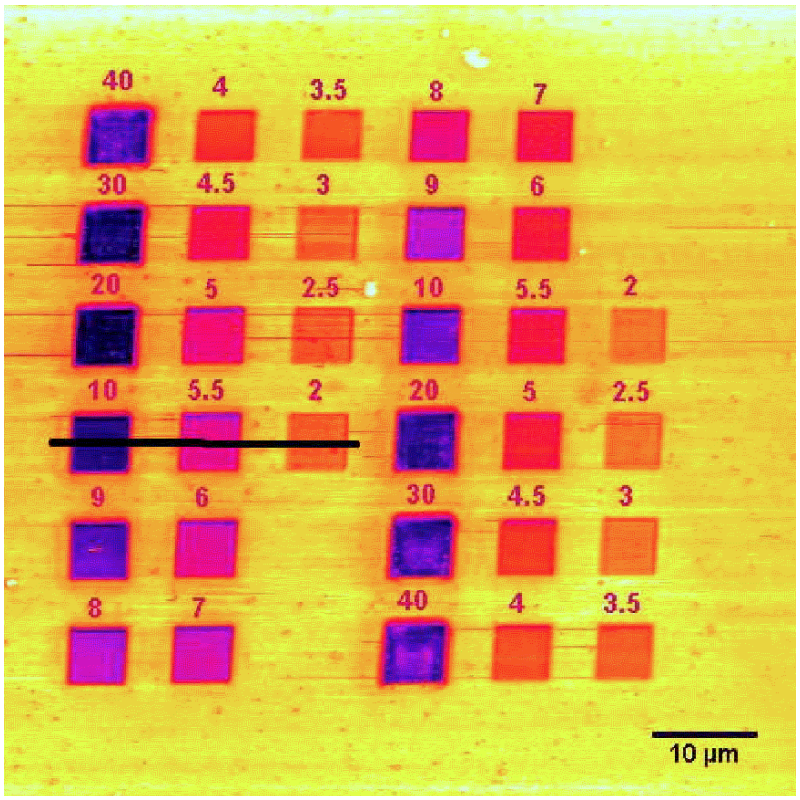

Figure 3.7 Topographic image of 5 µm^2 squares etched in PEDOT:PSS, demonstrating grayscale etching is possible by the incident laser power. The power (mW) used to etch the squares are written on top of each region.

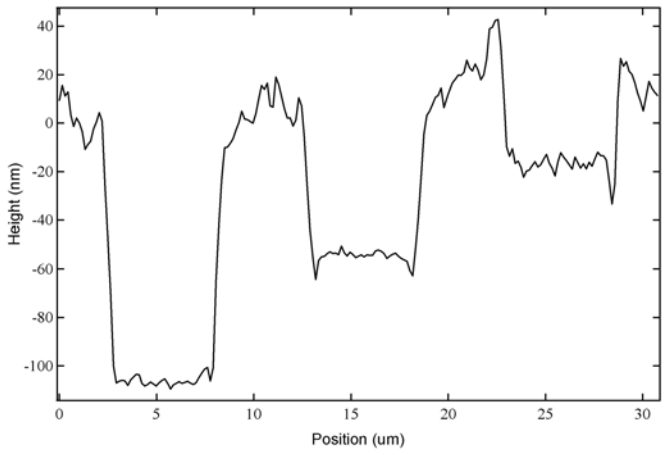

Figure 3.8 Line profile designated by the black line in Figure 3.7.

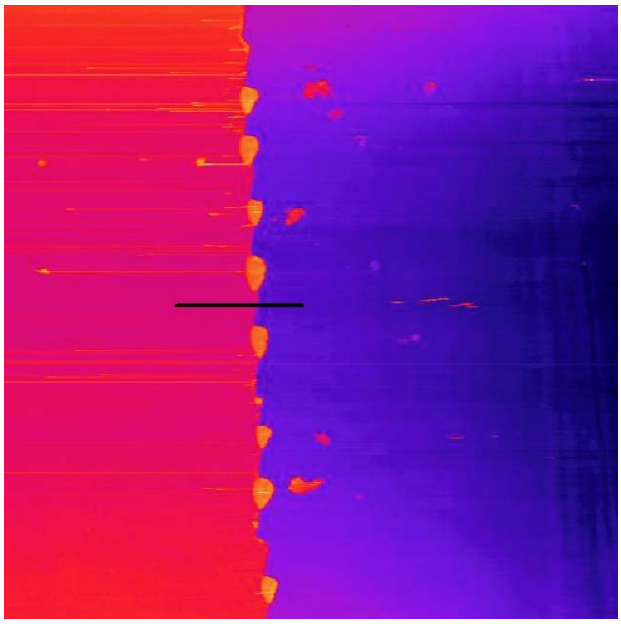

Figure 3.9 An AFM image of a scratched film used to determine film thickness.

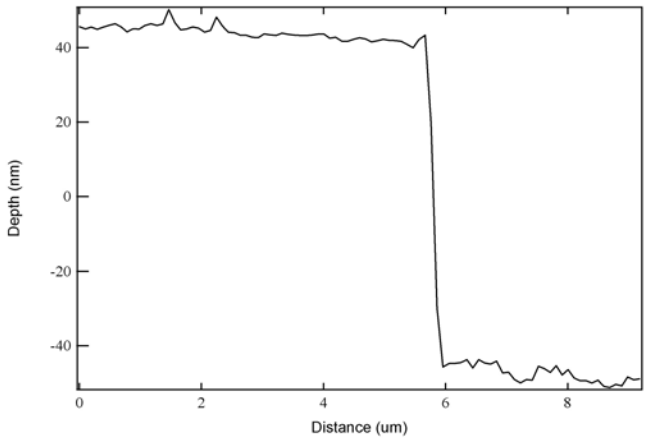

Figure 3.10 The line profile of the black line shown in Figure 3.9.

.

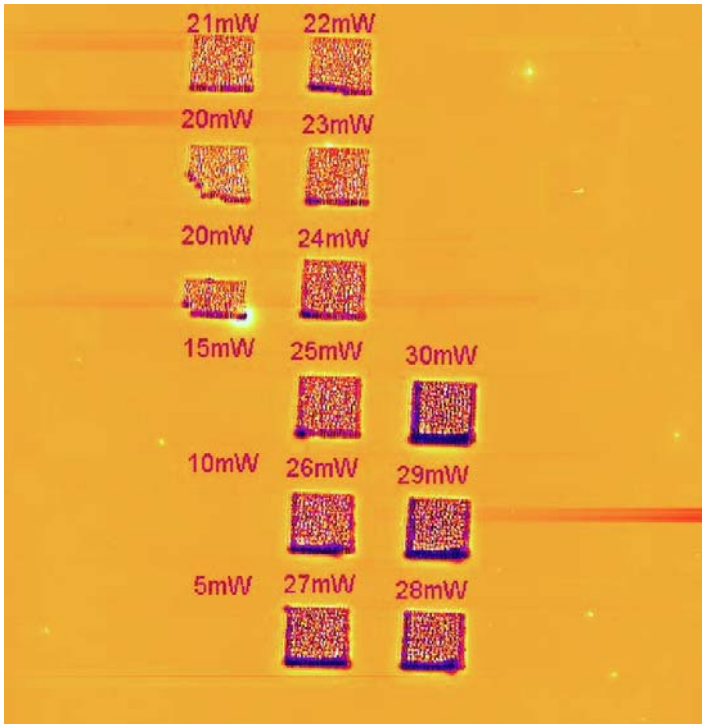

Figure 3.11 Topographic image of 5 μm^2 squares etched in a PSS film. The power with which the regions were etched are shown above each square.

Both of these observations are consistent with PSS etching by a higher order nonlinear optical process than in the case of PEDOT:PSS.

3.3.2 Quantitative Model for Power Dependence Etching

Quantitative information on the nonlinear nature of etching can be obtained from the power dependent etching data shown above[42]. First, by modeling multiphoton etching as a simple kinetic process, in which etching is assumed to occur by multiphoton induced depolymerization of the polymer, one can write:

Polymer + n Photons → m Fragments (1)

Next, supposing the kinetics are first order in the polymer concentration, C_{poly}, the rate of polymer decomposition can be written as:

$$\frac{d\ C_{poly}}{dt} = k\, C_{poly} P^n \qquad (2)$$

where n is the order of the optical absorption process, P is the photon flux which is directly proportional to the incident power, k is the rate constant, and t is time. After etching the film for time τ at a given power P, integration of equation (2) leads to following expression:

$$C_{poly}(t, P) = C_{poly}(0) \exp(ktP^n) \qquad (3)$$

$C_{poly}(0)$ is the initial polymer concentration before etching. The irradiation time τ is not simply the pixel time, but rather a multiple of it depending on the number of times a specific sample region has been scanned through. By relating polymer concentration to the film etch depth, $D_{poly}(\tau,P)$, when $D_{poly}(0)$ is the unetched film thickness:

$$D_{poly}(t,P) = D_{poly}(0)\left[1 - \exp(-ktP^n)\right] \qquad (4)$$

Plugging in the data of Figures 12 a and b to Equation (4) yields kt=0.08±0.01, and n=1.5±0.1, for PEDOT:PSS, and kt=2 x 10^{-6}, n=5±1 for PSS. For nonlinear systems, the value of n is the primary factor governing the slope of the etch depth vs. incident power plot in the transition region where powers are above threshold but below saturation. On the other hand, the value of kt has a main effect on the "threshold" for nonlinear etching processes. All other sets of data show the same kt and n values within experimental and curve fitting errors, so these data are very reliable and reasonable.

3.3.3.Comparison of PEDOT:PSS and PSS Etching Results

Comparison of the above etching results indicates that PEDOT:PSS is much more easily etched than PSS alone. In fact, the data shown in Figure 3.12 (a) and (b) indicate that PEDOT:PSS etching is almost complete (i.e. the film has been almost fully removed) prior to the onset of PSS film etching. This result was not initially expected, given that the majority component of the PEDOT:PSS used is PSS. The fact that PEDOT:PSS etching apparently occurs by a lower order process than PSS etching alone indicates that PEDOT may serve as a sensitizer for PSS etching[100-102]. Specifically, radical formation during depolymerization of PEDOT may lead to enhanced etching of the PSS component in the mixed films. Alternatively, PEDOT:PSS etching may rely more heavily on photothermal processes, while PSS etching is driven primarily by a photochemical mechanism. Such a difference in mechanisms is qualitatively consistent with the different electronic absorption spectra of these materials, with PEDOT:PSS absorbing relatively low energy photons compared to PSS.

Another important confirmation that ablation involves a multiphoton process is that the film is not etched at all with the laser operating under CW mode. The only difference between continuous wave and mode lock for the laser system is the latter produces high intensity laser pulses in a ultra short time interval, 170 femtosecond in this thesis. Under this condition, several photons could be absorbed by the polymeric chromophores at the same time. An AFM image showing etching results at 9 and 10 mW under CW and pulsed laser operation is shown in Figure 3.13.

3.4 Etching of Grayscale Patterns in PEDOT:PSS

Etching of three-dimensional surface relief (grayscale) structures in PEDOT:PSS films is readily achieved by varying the power of the incident 870 nm light, as evidenced by the data shown in Figure 3.7. While complete removal of the film requires average incident powers greater than 10 mW (Figure 3.7), this film could be etched to ~50% of its depth using 5 mW and ~20% of its depth at 2 mW. Partially etched film regions are often relatively smooth, exhibiting RMS roughness of 4.165 nm. This roughness corresponds favorably to the roughness of the

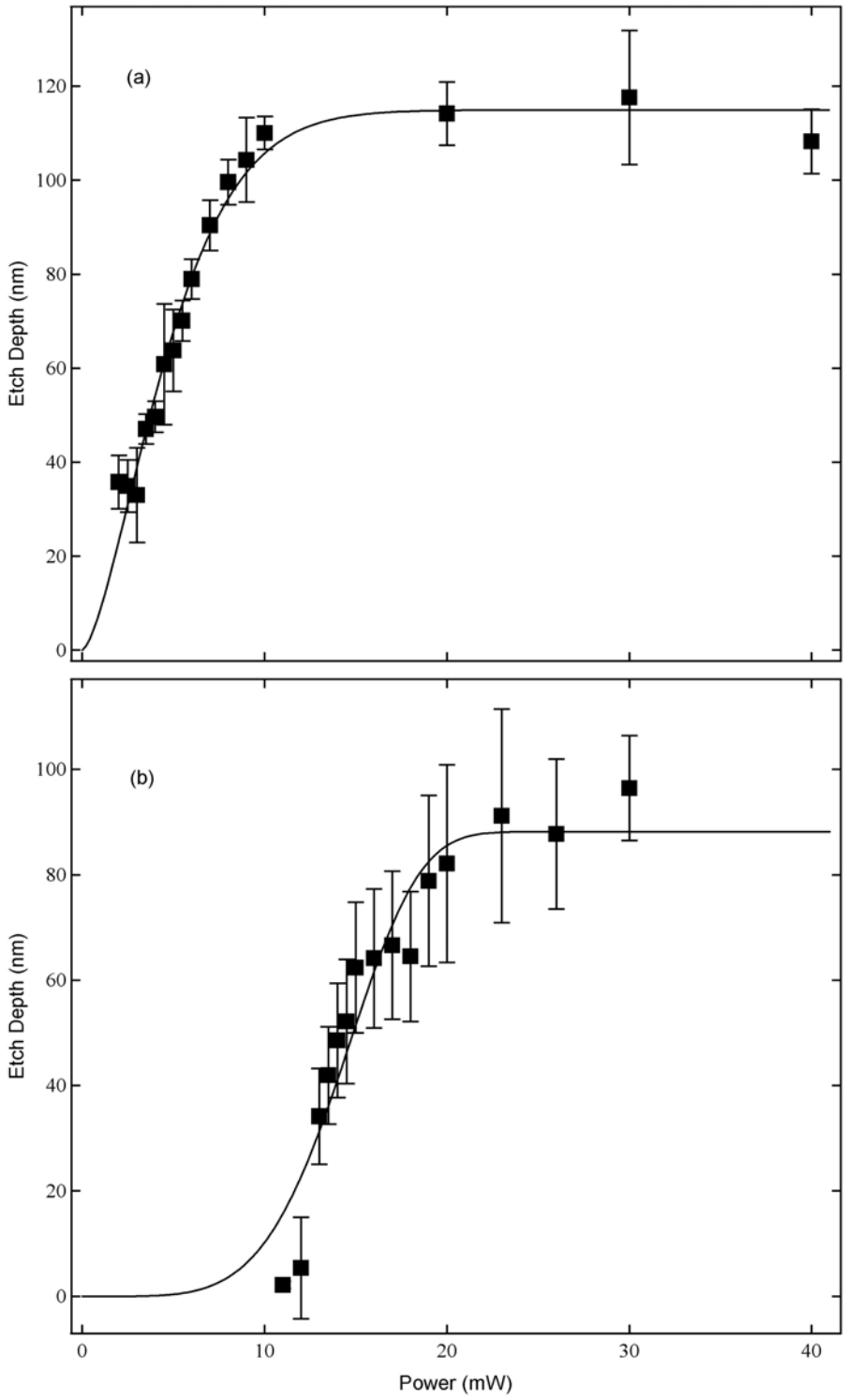

Figure 3.12 Data fitting of PEDOT:PSS (a) and PSS alone (b) power dependence.

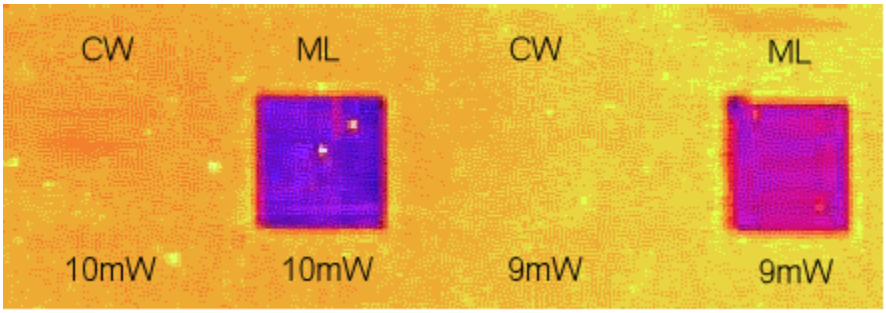

Figure 3.13 Etching at 9 and 10 mW under mode-locked and continuous-wave modes of the laser.

original unetched film (1.032 nm RMS roughness). Unfortunately, our current instrument does not allow for rapid modulation of the incident laser power for the purpose of grayscale etching. So instead, grayscale structures were prepared by modulating the laser focus in the present study. Laser focus modulation provides an effective means to vary the incident energy flux and hence, the local etch depth.

In all of these studies, the optimum initial focus of the laser was determined by recording the fluorescence from the film as a function of the objective position, as describe above. Variation of the incident photon flux and etch rate was then accomplished by moving the focus position off the optimum focus in a controlled fashion. The dependence of etching on the focal position can be predicted using Equation (4) and (5), and the experimental parameters determined by fitting the power-dependent etch data depicted in Figure 3.12 (a). In the case of focus-dependent etching, the photon flux, P, becomes P(z) and is dependent on the laser focus position (z). P(z) follows a Lorentzian profile[98]:

$$P(z) = \frac{P_{max}}{1 + (\frac{z\lambda}{\pi w_0})^2} \qquad (5)$$

Where $w_0 = 0.41\lambda/NA$ is the beam waist, λ is the wavelength of the incident light, NA is the numerical aperture of the microscope objective and P_{max} is the maximum energy flux when the laser is focused within the film.

To test the expected dependence of etch depth on the laser position, 5 μm^2 regions were etched into PEDOT:PSS films in a manner similar to the power dependent etching experiments. Nevertheless in this case, the incident average power stayed the same for all squares, while the microscope focus position was changed by a computer-controlled piezo-electric objective mount. Figure 3.14 depicts an AFM image showing the results obtained from one such experiment. Etching in this case was performed at 20 mW. Figure 3.15 plots a line profile taken from these data, and as expected, the etch depth clearly varies with focus position. The average etch depths in each etched region were determined from these data and were plotted as a function of focus position in Figure 3.16. The error bars on the data points reflect the RMS roughness measured in each region.

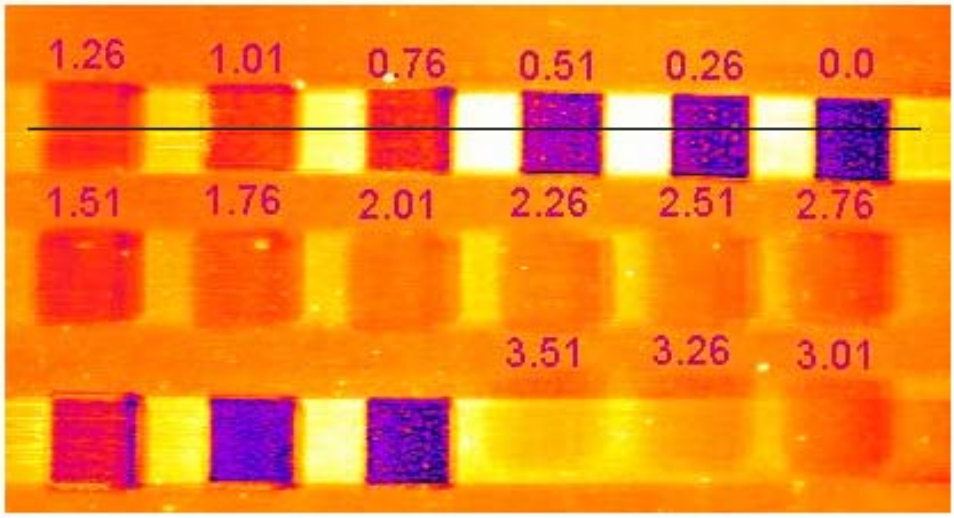

Figure 3.14 AFM image showing the focus dependence of PEDOT:PSS film etching. Each square region (5 x 5 μm^2) was etched at 20 mW incident power (40 ms irradiation, 100 nm pixels) at the focus position (μm) designated on the image. The focus position is given relative to the film center, as determined in Figure 3.3.

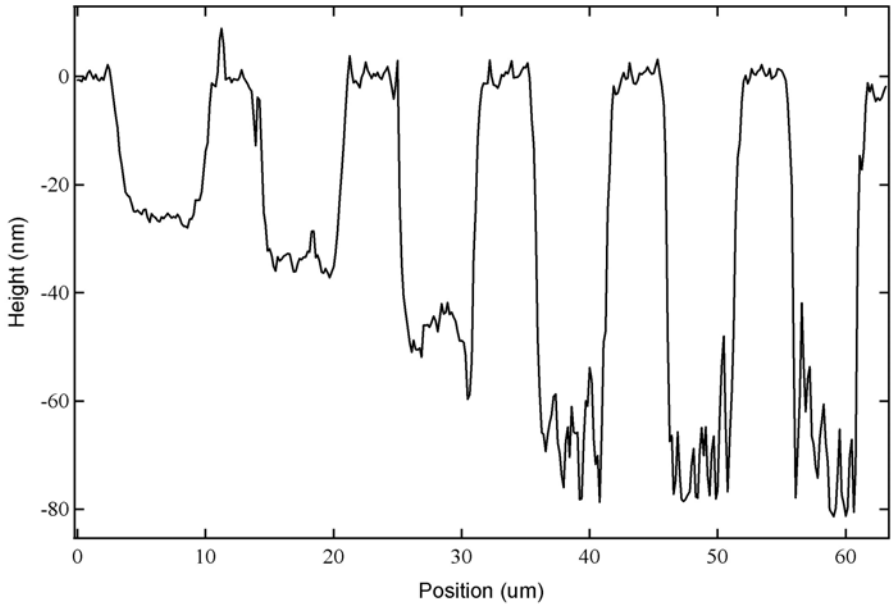

Figure 3.15 Line profile designated by the black line in Figure 3.14.

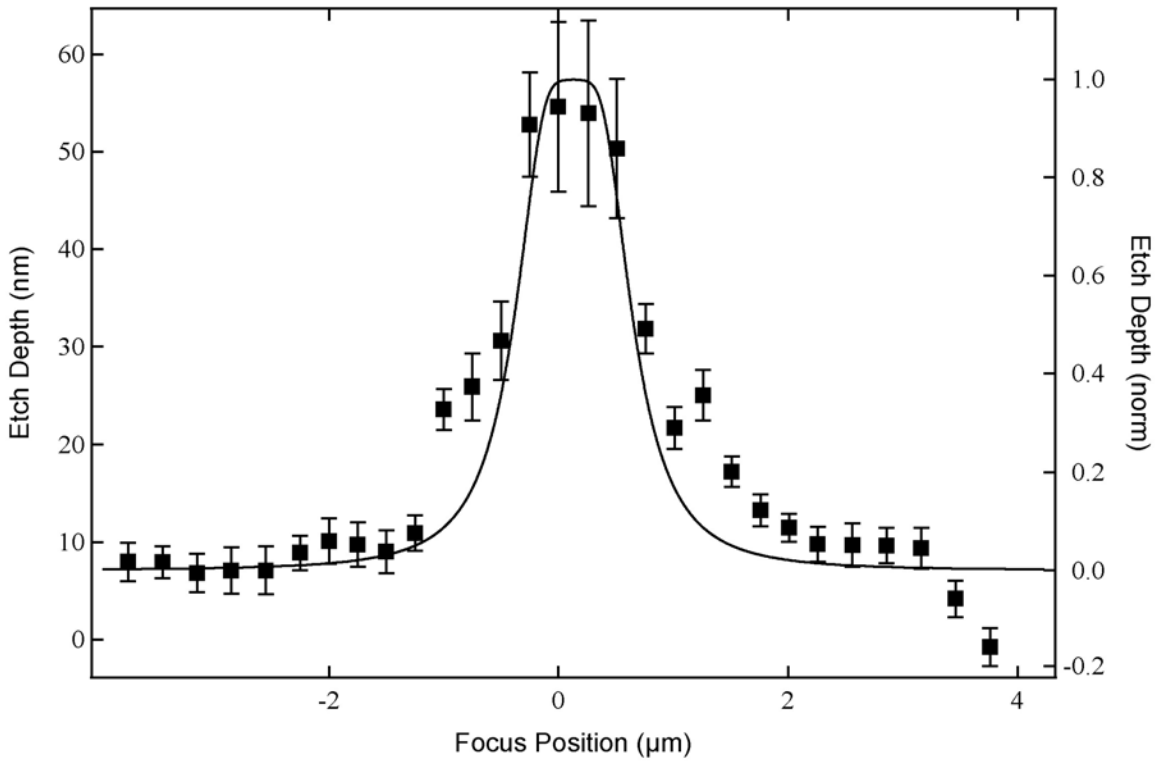

Figure 3.16 Average etch depth (squares) as a function of focus position along the thickness direction. The value shown and the error bars were determined from three replicate experiments, and the solid line shows the curve expected for an etching process defined by the kinetic parameter obtained from Figure 3.15. The expected curve fits reasonably well to the experimental data.

Importantly, the solid line plotted across the data in Figure 3.16 is not a fit to the data, but rather, it plots the normalized etch depth expected based on the model described in Equations (4) and (5), employing $n = 1.5$ and $k\tau = 0.08$. The experimental data follow the model reasonably well near the focus of the microscope. However, even with the microscope far out of focus, a small amount of residual etching occurs that is not explained by the present model. The precise reason for this out-of-focus etching is unclear at present. It may result from aberrations in the optical systems that lead to sub-optical focus characteristics. It may also be a reflection of participation of a totally different etching mechanism involving direct heating of the polymer by one photon absorption of the incident laser light. However, the dominant etching process observed is explained well by the model from Equations (4) and (5). And this model was used to properly position the laser focus for each gray level during the etching of grayscale patterns under incident powers of 20 mW or higher.

Figure 3.17 depicts a grayscale template (a pyramid) used to etch pyramidal features into PEDOT:PSS films, along with AFM images obtained from the etched films. Figure 3.18 B)-D) depict AFM images obtained from pyramids etched at 5 mW, 20 mW and 30 mW. In all three cases, the AFM images clearly show pyramidal structures which are close to the template. Figure 3.18 E) plots line profiles taken horizontally across central portions of the pyramids shown in Figure 3.17 B)-D). These lines are plotted on the same scale to depict differences in the etch depths. The pyramids etched at 20 and 30 mW encompass approximately the full depth of the film. These pyramids exhibit somewhat greater topographic roughness than does the pyramid etched at 5 mW, due to the presence of etching debris in the former. Such debris is routinely observed when films are etched at powers near or just above saturation and is attributed here to a residual preference for etching of PEDOT over PSS.

The pyramid etched at 5 mW clearly demonstrates that three-dimensional surface relief structures can be prepared with high precision. The RMS roughness of the sloped portions of the pyramid shown in Figure 3.17 B) is 1.0 ± 0.8 nm, revealing that ~ 20 nm tall structures can be etched with 1 nm precision. As a final demonstration, Figure 3.17 F) depicts a spiral ramp etched into PEDOT:PSS at 20 mW incident power. The film height within this latter structures varies linearly over a height range of 45 nm. Significantly less debris is formed because the laser was moved off the optimal focus relatively rapidly during etching of this pattern. As a result, 2 ± 2 nm RMS roughness is observed within the etched region.

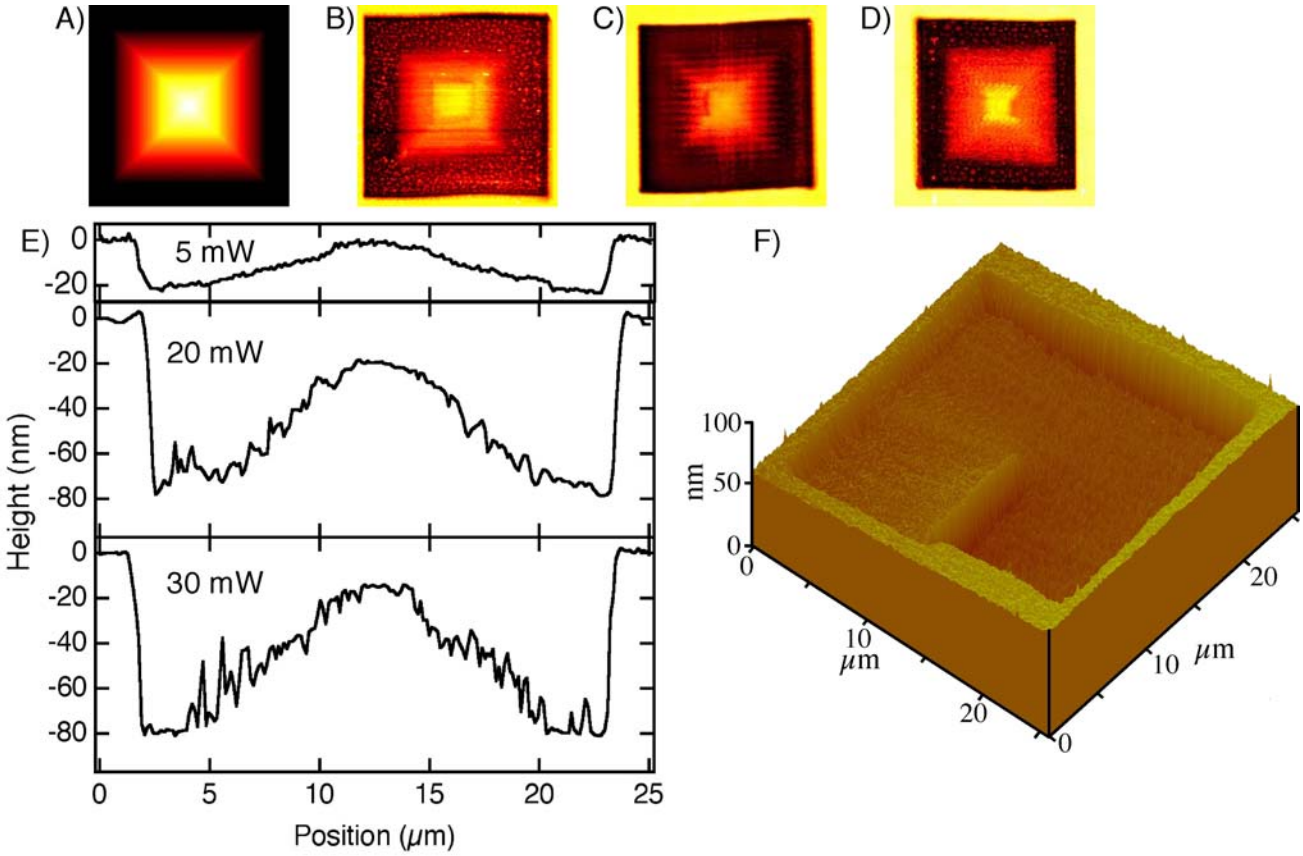

Figure 3.17 Grayscale structures fabricated by ablative multiphoton photolithography. The grayscale template (a pyramid surrounded by a flat region) used in the microscope control software is shown in A). AFM images of pyramids etched into thin PEDOT:PSS films are shown in B) (5 mW), C) (20 mW), and D) (30 mW). Line profiles taken across the center of each pyramid are shown in E). A spiral ramp etched into a PEDOT:PSS film at 20 mW is shown in F). The mean RMS roughness of the pyramid shown in b was determined to be 1.0 nm (± 0.8 nm) while the spiral ramp yielded a mean roughness of 2 nm.

CHAPTER 4 - Conclusion and Future Work

The controlled etching of grayscale relief structures into technologically-important PEDOT:PSS thin films has been demonstrated, using ablative multiphoton photolithography with a near-IR femtosecond pulse laser. The data show that grayscale structures can be prepared in thin (~ 80 nm) films with a remarkable precision of ~ 1 nm when the films are etched to a fraction of their full thickness. PEDOT:PSS films were found to be etched by a low order nonlinear optical process, which facilitated grayscale patterning. A simple kinetic model for the etching process was used to precisely position the laser focus during the fabrication of grayscale structures. Etching of grayscale surface relief structures by ablative multiphoton methods has important potential applications in the fabrication of organic electronic devices[25]. It may also serve as a new means to prepare high resolution optical and optoelectronic devices[24], such as those based on polymer-dispersed liquid crystals[92], and to fabricate nanofluidic devices[26].

Etching process of PEDOT:PSS, believed to be a combination of linear and nonlinear processes, causes debris. This debris is explained as the residual preference for etching PEDOT over PSS. Future studies of other conducting polymers will be focused on single component materials in order to eliminate such debris. As demonstrated in experimental section, grayscale patterns are also possibly produced by modulating the incident power. So it would be promising to accomplish grayscale etching by precisely controlling the power of the incident light. Other than the grayscale patterns fabricated in this thesis, more complicated features should be produced based on the present experimental setup. Therefore, laser ablation technique could be used to produce more applicable structures, such as, use this technique to fabricate complex channel structures inside of polymers for microfluidic devices.

References

1. Heuberger, A.; Bruenger, W. *Microelec. Eng.* **1966**, *34(1)*, 39-50.
2. Sotomayor, T.; Clivia, M. *Fundamentals. Nanoelec.* **2003**, *14*, C1/1-C1/18.
3. Nikolaus, B.; Patlo, W. N.; Fomenkov, I. V. *Solid. State. Technol.* **2002**, *45(2)*, 43-44, 46, 48.
4. Crozatier, C.; Berre, M. Le.; Chen, Y. *Microelec. Eng.* **2006**, *83(4-9)*, 910-913.
5. Rothschild, M. *Mater. Today.* **2005**, 18-24.
6. Orlowski, M.; Wild, A. *ECS. Trans.* **2006**, *3(6)*, 3-17.
7. Wu, B. Q.; Kumar, A. *J. Vac. Sci. Technol.* **2007**, *B25(6)*, 1743-1761.
8. Spitzer, R. C.; Kauffman, L. R.; Orzechowski, T.; Phillion, D. W.; Cerjan, C. *J. Vac. Sci. Technol.* **1993**, *B11*, 2986-2989.
9. Kubiak, G. D.; Berger, K. W.; Haney, S. J.; Rockett, P. D,; Hunter, J. A. OSA. *Proc. Soft. X-ray. Projection. Lithog.* **1993**, *18*, 127-131.
10. Skulina, K.; Alford, C.; Bionta, R.; Makowiecki, D.; Gullikson, E. M.; Soufli, R.; Kortright, J. B.; Underwood, J. H. *OSA Proc. Extreme. Ultraviolet. Lithog.* **1995**, *23*, 52-55.
11. Chou, S. Y.; Krauss, P. R.; Renstrom, P. J. *J. Vac. Sci . Technol.* **1996**, *B14(6)*, 4129-4131.
12. Maruo, S.; Kawata, S. J. *Microelectromech. Sys.* **1998**, *7*, 411-415.
13. Sun, H. B.; Kawakami, T.; Xu, Y.; Ye, J. Y.; Matuso, S.; Misawa, H.; Miwa, M.; Kaneko, R. *Opt. Lett.* **2000**, *25(15)*, 1110-1112.
14. Sun, H. B.; Matuso, S.; Misawa, H. *Appl. Phys. Lett.* **1999**, *74*, 786-788.
15. Cumpston, B. H.; Ananthavel, S. P.; Barlow, S.; Dyer, D. L.; Ehrlich, J. E.; Erskine, L. L.; Heikal, A. A.; Kuebler, S. M.; Lee, Y. S.; McCord, M. D.; Qin, J.; Rockel, H.; Rumi, M.; Xu, X. L.; Marder, S. R.; Perry, J. W. *Nature.* **1999**, *398*, 51-54.
16. Kawata, S.; Sun, H. B.; Tianka, T.; Takada, K. *Nature.* **2001**, *412*, 697-698.
17. Ovsianikov, A.; Ostendort, A.; Chichkov, B. N. *Appl. Surf. Sci.* **2007**, *253(15)*, 6599-6602.
18. Radhakrishnan, G.; Adams, P. M.; Bernstein, L. S. *Appl. Surf. Sci.* **2007**, *253(19)*, 7651-7655.
19. Loeffler, M.; Ruemmeli, M. H.; Kramberger, C.; Borowiak-Palen, E.; Klingeler, R.; Gemming, T.; Beuchner, B.; Pichler, T. *Chem. Mater.* **2008**, *20(1)*. 128-134.
20. Xiao, Y. W.; Guo, M. S.; Zhang, P.; Shanmugam, G.; Polavarapu, P.; Huston, M. S. *Biophys. J.* **2008**. *94(4)*, 1359-1366.

21. Pfleging, W.; Bruns, M,; Welle, A.; Wilson, S. *Appl. Surf. Sci.* **2007**, *253(23)*, 9177-9184.
22. Becker, J. S.; Zoriy, M.; Becker, J. S.; Dobrowolska, J.; Matusch, A. *J. Anal. Atomic. Spectro.* **2007**, *22(7)*, 736-744.
23. Costello, A.; Sears, J. *Laser Institute of America (Publications).* **2006**, *99*, 139-143.
24. Ismail, R. A.; Hassan, K. I.; Abdulrazaq, O. A.; Wesam, H. *Mater. Sci. Semicond. Process.* **2007**, *10(1)*, 19-23.
25. Kim, D.; Jeong, S.; Moon, J.; Han, S.; Chung, J. *Appl. Phys. Lett.* **2007**, *91(7)*, 071114/1-071114/3.
26. Yuan, D. J.; Das, S. *J. Appl. Phys.* **2007**, *101(2)*, 024901/1-024901/6.
27. Srinivasan, R.; Mayne-Banton, S. *Appl. Phys. Lett.* **1983**, *41*, 576-578.
28. Kawamura, Y.; Toyoda, K.; Namba, S. *Appl. Phys. Lett.* **1983**, *40*, 374-375.
29. Patel, R. S.; Wassick, T. A. *Proc. SPIE-int. Soc. Opt. Eng.* **1997**, *2991*, 217-223.
30. Aoki, H. *U.S. Patent 5736999*, **1998**.
31. Arnold, N.; Luk'yanchuk, B.; Bityurin, N. *Appl. Surf. Sci.* **1998**, *127*, 184-192.
32. Lazare, S.; Granier, V. *Laser. Chem.* **1989**, *10*, 25-40.
33. Bauerle, D. *Laser Processing and Chemistry, Third Edition.* Springer-Verlag. Berlin, **2000**.
34. Lippert, T.; Kunz, T.; Hahn, C.; Wokaun, A. *Recent. Res. Devel. Macromol. Res.* **1997**, *2*, 121-142.
35. Lippert, T.; Dickinson, J. T. *Chem. Rev.* **2003**, *103*, 453-485.
36. Bachman, F. *Chemtronics.* **1989**, *4*, 149-152.
37. Srinivasan, R. *Appl. Phys. A.* **1993**, *56*, 417-423.
38. Masabuchi, T.; Tada, T.; Nomura, E.; Hatanaka, K.; Fukumura, H.; Masuhara, H. *J. Phys. Chem. A.* **2002**, *106*, 2180-2186.
39. Ball, Z.; Hopp, B.; Csete, M.; Ignacz, F.; Racz, B.; Szabo, G.; Szabo, G. *Appl. Phys. A.* **1995**, *61*, 575-578.
40. Ortelli, E. E.; Geiger, F.; Lippert, T.; Wei, J.; Wokaun, A. *Macromolec.* **2000**, *33*, 5090-5097.
41. Ortelli, E. E.; Geiger, F.; Lippert, T.; Wokaun, A. *Appl. Spectro.* **2001**, *55*, 412-419.
42. Ibrahim, S.; Higgins, D. A.; Ito, T. *Langmuir.* **2007**, *20*, 12406-12412.
43. Kueper, S.; Stuke, M. *Appl. Phys. A.* **1989**, *49(2)*, 211-215.
44. Srinivasan, R.; Braren, B.; Casey, K. G.; Yeh, M. *J. Appl. Phys.* **1990**, *68*, 1842-1847.
45. Lippert, T.; Webb, R. L.; Langford, S. C. *J. Appl. Phys.* **1999**, *85*, 1838-1847.

46. Lippert, T.; Webb, R. L.; Langford, S. C. *J. Appl. Phys.* **1999**, *85*, 1838-1847.

47. Lippert, T.; Stebani, J.; Ihlemann, J.; Nuyken, O.; Wokaun, A. Angew. *Makromol. Chem.* **1993**, *213*, 127-155.

48. Davis, C. R.; Snyder, R. W.; Egitto, F. D.; D'Couton, G. C.; Babu, S. V. *J. Appl. Phys.* **1994**, *76*, 3049-3051.

49. Lippert, T.; Yabe, A.; Wokaun, A. *Adv. Mater.* **1997**, *9*, 105-119.

50. Vasilets, V. N.; Yuranova, T. I.; Ponomarev, A. N. *J. Photopolym. Sci. Technol.* **1994**, *7*, 309-314.

51. Fuchs, F.; Goetzberger, O.; Henck, R.; Fogarassy, E. *Appl. Phys. A.* **1995**, *60*, 505-507.

52. Shinozuka, T.; Shirai, M.; Tsunooka, M. *J. Photopolym. Sci. Technol.* **2000**, *13*, 751-757.

53. Murahara, M. M.; Funatsu, T.; Okamoto, Y. *Proc. SPIE-int. Soc. Opt. Eng.* **2005**, *5647*, 224-231.

54. Davis, G. M.; Gower, M. C. *J. Appl. Phys.* **1987**, *61(5)*, 2090-2092.

55. Rebollar, E.; Bounos, G.; Oujja, M.; Domingo, C.; Georgiou, S.; Castillejo, M. *J. Phys. Chem. B.* **2006**, *110(29)*, 14215-14220.

56. Srinivasan, R. *J. Appl. Phys.* **1991**, 70(12), 7588-7593.

57. Bozhevolnyi, S. I.; Potemkin, I. V.; Svetovoy, V. B. *J. Appl. Phys.* **1992**, *71*, 2030-2032.

58. Kumagai, H.; Midorikawa, K.; Toyoda, K.; Nakamura, S.; Okamoto, T.; Obara, M. *Appl. Phys. Lett.* **1994**, *65*, 1850-1852.

59. Srinivasan, R.; Sutcliffe, E.; Braren, B. *Appl. Phys. Lett.* **1987**, *51*, 1285-1287.

60. Kuper, S.; Stuke, M. *Appl. Phys. B.* **1987**, *44*, 199-204.

61. Kuper, S.; Stuke, M. *Appl. Phys. Lett.* **1989**, *54*, 4-6.

62. Preuss, S.; Spath, M.; Zhang, Y.; Stuke, M. *Appl. Phys. Lett.* **1993**, *62*, 3049-3051.

63. Vogel, A.; Venugopalan, V. *Chem. Rev.* **2003**, *103*, 577-644.

64. Elvers, D.; Remer, L.; Arnold, N.; Bauerle, D. *Appl. Phys. A.* **2005**, *80*, 55-59.

65. Georgiou, S. *Adv. Polym. Sci.* **2004**, *168*, 1-49.

66. Chrisey, D. B.; Pique, A.; McGill, R. A.; Horwitz, J. S.; Ringeisen, B. R.; Bubb, D. M.; Wu, P. K. *Chem. Rev.* **2003**, *103*, 553-576.

67. Gritsenko, K. P.; Krasovsky, A. M.; *Chem. Rev.* **2003**, *103*, 3607-3649.

68. Dreisewerd, K. *Chem. Rev.* **2003**, *103*, 395-426.

69. Karas, M.; Kruger, R. *Chem. Rev.* **2003**, *103*, 427-440.

70. Knochemnuss, R.; Zenobi, R.; *Chem. Rev.* **2003**, *103*, 441-452.

71. Bubb, D. M.; O'Malley, S. M.; Antonacci, C.; Simonson, D.; McGill, R. A. *J. Appl. Phys.* **2004**, *95*, 2175-2177.

72. Georgiou, S.; Koubenakis, A. *Chem. Rev.* **2003**, *103*, 349-393.

73. Snelling, H. V.; Walton, C. D.; Whitehead, D. *J. Appl. Phys. A.* **2004**, *79*, 937-940.

74. Van Steenberge, G.; Geerinck, P.; Van Put, S.; Van Koetsem, J.; Ottevaere, H. Morlion, D.; Thienpont, H.; Van Daele, P. *J. Lightwave. Technol.* **2004**, *22*, 2083-2090.

75. Rubahn, K.; Ihlemann, J.; Jacopic, G.; Simonsen, A. C.; Rubahn, H. G. *Appl. Phys. A.* **2004**, *79*, 1715-1719.

76. Gozzini, A.; Mango, F.; Xu, J. H.; Alzetta, G.; Maccarrone, F.; Bernheim, R. A.; *Nuovo. Cimento. D.* **1993**, 15, 709-722.

77. Womack, M.; Vendan, M.; Molian, P. *Appl. Surf. Sci.* **2004**, *221*, 99-109.

78. McDonald, J. P.; Hendricks, J. L.; Mistry, V. R.; Martin, D. C.; Yalisove, S. M. *J. Appl. Phys.* **2007**, *102*, 013107/1-013107/5.

79. Liang, X. F.; Chen, Y.; Chen, L.; Yin, J.; Liu, Z. G. *Appl. Phys. Lett.* **2007**, *90(2)*, 022508/1-022508/3.

80. Morandi, V.; Marabelli, F.; Amendola, V.; Meneghetii, M.; Comoretto, D. *Adv. Funct. Mater.* **2007**, *17(15)*, 2779-2786.

81. Huang, S. M.; Hong, M. H.; Wu, D. J.; Van, L. H.; Ong, T. S.; Luk'yanchuk, B. S.; Chong, T. C. *Proc. SPIE-int. Soc. Opt. Eng.* **2003**, *5069*, 264-268.

82. Sasaki, J.; Youoku, S.; Tamamushi, K.; Ito, A. *Proc. SPIE-int. Soc. Opt. Eng.* **2005**, *5718*, 186-193.

83. Ouyang, J. Y.; Chu, C. W.; Chen, F. C.; Xu, Q. F.; Yang, Y. *J. Macromolec. Sci. Pure. Appl. Chem.* **2004**, A41(12), 1497-1511.

84. Lin, S. T.; Chang, M. H.; Horng, J. B.; Cheng, H. L.; Chou, W. Y. *Proc. SPIE-int. Soc. Opt. Eng.* **2007**, 66551N/1-66551N/11.

85. Andersson, P.; Forchheimer, R.; Tehrani, P.; Berggren, M. *Adv. Funct. Mater.* **2007**, 17(16), 3074-3082.

86. Yan, H.; Kagata, T.; Mori, Y.; Harashina, Y.; Hara, Y.; Okuzaki, H. *Chem. Lett.* **2008**, 37(1), 44-45.

87. Hains, A. W.; Marks, T. J. *Appl. Phys. Lett.* **2008**, 92(2), 023504/1-023504/3.

88. Mu, H.; Li, W.; Jones, R.; Steckl, A.; Klotzkin, D. *J. Lumine.* **2007**, *126(1)*, 225-229.

89. Vacca, P.; Petrosino, M.; Miscioscia, R.; Nenna, G.; Minarini, C.; Della Sala, D.; Rubino, A. *Thin. Solid. Films.* **2006**, *516(12)*, 4232-4237.

90. Wang, X. J.; Ostblorn, M.; Johansson, T.; Inganas, O. *Thin. Solid. Films.* **2004**, *449*, 125-132.

91. Spielmann, C.; Burnett, N. H.; Sartania, S.; Kippitsch, R.; Schnurer, M.; Kan, C.; Lenzner, M.; Wobrauschek, P.; Krausz, F. *Science*. **1997**, 278(5338), 661-664.

92. Higgins, D. A.; Everett, T. A.; Xie, A.; Forman, S. M.; Ito, T. *Appl. Phys. Lett.* **2006**, *88*, 184101/1-184101/3.

93. Kirchmeyer, S.; Reuter, K. J. *Mater. Chem.* **2005**, *15*, 2077-2088.

94. Arias, A. C.; Granström, M.; Thomas, D. S.; Petritsch, K.; Friend, R. H. *Phys. Rev. B.* **1999**, *60*, 1854-1860.

95. Brown, T. M.; Kim, J. S.; Friend, R. H.; Cacialli, F.; Daik, R.; Feast, W. J. *Appl. Phys. Lett.* **1999**, *75*, 1679-1681.

96. de Kok, M. M.; Buechel, M.; Vulto, S. I. E.; van de Weijer, P.; Meulenkamp, E. A.; de Winter, S. H. P. M.; Mank, A. J. G.; Vorstenbosch, H. J. M.; Weijtens, C. H. L.; van Elsbergen, V. *Phys. Stat. Sol. A.* **2004**, *201*, 1342-1359.

97. Sirringhaus, H.; Kawase, T.; Friend, R. H.; Shimoda, T.; Inbasekaran, M.; Wu, W.; Woo, E. P. *Science.* **2000**, *290*, 2123-2126.

98. Demtröder, W. Laser Spectroscopy: *Basic Concepts and Instrumentation*; Springer-Verlag: Berlin, **1996**.

99. Grzybowski, B. A.; Haag, R.; Bowden, N.; Whitesides, G. M. *Anal. Chem.* **1998,** *70*, 4645-4652.

100. Lippert, T.; Dickinson, J. T. *Chem. Rev.* **2003**, *103*, 453-485.

101. D'Couto, G. C.; Babu, S. V.; Egitto, F. D.; Davis, C. R. *J. Appl. Phys.* **1993**, *74*, 5972-5980.

102. Grzybowski, B. A.; Haag, R.; Bowden, N.; Whitesides, G. M. *Anal. Chem.* **1998**, *70*, 4645-4652.